Microstructural analysis on experimentally sheared limestone gouge
What causes velocity weakening?

Master Thesis, August 2010

Resi Veeningen BSc

University of Utrecht
Faculty of Geosciences
HPT-group / SG&T-group

Universiteit Utrecht

Table of Contents

Abstract

A recent experimental study on fault gouges prepared from limestone samples taken from the Longmen Shan Fault Zone, which hosted the Great Wenchuan Earthquake of 2008, showed unstable, velocity weakening slip in low velocity experiments performed at temperatures of 100-150°C but stable, velocity strengthening slip at lower temperatures. Velocity weakening is the process of shear strength reduction with increasing sliding velocities and is a requirement for seismogenesis. The frictional properties were studied macroscopically with help of the Rate and State dependent Friction law. However, the resulting data do not enable identification of the microphysical processes which cause velocity weakening in the limestone gouge. To determine the process causing velocity weakening, the simulated fault gouge has been examined under the light and electron microscope, with magnifications ranging from 5 to 150.000 times. Calcite twins and fractures were observed and the density of these structures seems to increase with temperature. The 150°C limestone sample shows a more chaotic microstructure, with the R-shear bands being less common, broader and less recognizable compared to the 25°C-100°C sheared limestone gouges. Calcite twinning is also very common in the high temperature experiment. Quantitative analysis of the grain size distribution shows that the smallest grain sizes (minimum grain size ~50 nm) barely change whereas large polycrystalline clusters (~15 µm) do show a decrease in size. Comparison of the mechanical and microstructural data with previous microphysical models for the velocity dependence of slip suggests that possible microphysical reasons for velocity weakening includes competition between frictional viscous flow, dilatation, -and compaction due to granular rearrangement plus pressure solution and/or minor crystal plastic flow (twinning). The very small grain size developed in the samples might speed up processes like diffusion, allowing such mechanisms to control slip at relatively high rates.

1. Introduction

Figure 1 shows the Longmen Shan Fault Zone (LFZ), located in the Sichuan Province (southwestern China). It marks the eastern boundary of the Tibetan plateau by slipping the Longmen Shan Moutains in vertical direction. It caused the Great Wenchuan Earthquake (M_S 8.0) of May 12th 2008 which led to a tremendous amount of injuries and fatalities. To advance insights in the mechanics of earthquakes, scientists from several research groups have set up a large scale science plan shortly after the earthquake, in order to study the physical and mechanical properties of the LFZ fault rocks and protolithic sediments. The study of Verberne et al. (in press) formed a part of this plan with the study conducted here being the continuation of their results.

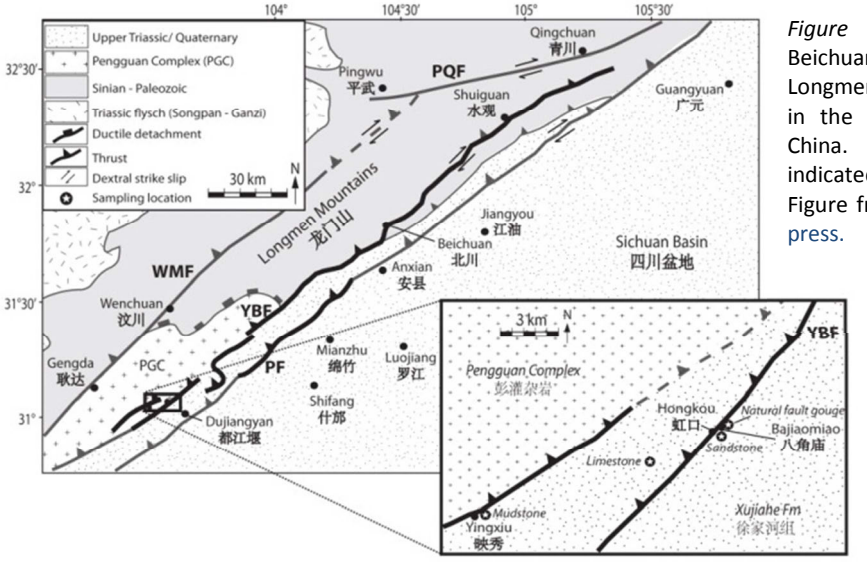

Figure 1: The Yingxiu – Beichuan portion of the Longmen Shan Fault Zone (LFZ) in the Sichuan province, SW China. Sample locations are indicated in the figure inset. Figure from Verberne et al., in press.

1.1. Background: Previous experiments on simulated limestone gouge from the LFZ

To investigate the rock friction properties of the lithologies located in and around the LFZ, laboratory experiments at the Institute of Geology of the CEA (Beijing) were conducted in 2009. Verberne et al. (in press) collected three different types of (intact) Upper Triassic sedimentary rock samples from the Xujiahe Formation, located at the southernmost part of the region affected by the earthquake (figure 1): (1) a limestone consisting of 95.8% calcite, (2) a carbonaceous sandstone and (3) a carbonaceous mudstone. Likewise, samples from the natural fault gouge were prepared for similar analysis. For the sample mineral content I refer to table 1 in Verberne et al. (in press). To produce a simulated fine grained and structureless, fault gouge, the sedimentary samples were crushed, ground, sieved (200 mesh sieve resulting in grain sizes up to 75 µm) and mixed into a paste. The fault gouge paste was sheared by axially shortening a saw-cut sample assembly consisting of an upper driver block (Fontainebleu sandstone) and a lower driving block (gabbro), sandwiching the gouge at an angle of 35° to the maximum stress. The complete set-up of the experiment is shown in figure 2. The samples were pressurized to 50MPa confining pressure (P_c) and 20 MPa pore pressure (P_p), corresponding to in-situ confining and hydrostatic pressures at a depth of ~2 km. Each material was sheared at four different temperatures: 25°C, 50°C, 100°C and 150°C, so that the effects of heat at depth and frictional heating during faulting was taken into account. Saw-cut displacement rates yields 1.22 µm/s with velocity steps of saw-cut displacement rates of 0.122 µm/s.

The frictional properties of the samples have been analysed quantitatively by Verberne et al. (in press). They discovered that the sandstone, mudstone and natural gouge show slip strengthening or steady state at all temperatures, with (steady state) friction coefficients (µ) of 0.3-0.4 for the natural gouge, and 0.5-0.6 for the sandstone and mudstone. This velocity strengthening behaviour was also observed in the low temperature (25°C and 50°C) simulated limestone gouge samples, showing friction coefficient values of ~0.7. However, at elevated temperatures (100°C and 150°C), the limestone gouge friction coefficient first peaked at a value of ~0.75 followed by significant slip weakening. This can be seen in figure 3. At 100°C, the limestone gouge showed steady state sliding behaviour at displacement rates of 1.22 µm/s and continuous slip weakening and strength oscillations when displacement rates were stepped to 0.122 µm/s. The limestone sheared at 150°C showed slip weakening after the peak strength, followed by on-going (stick-slip) oscillations independent on the displacement rate.

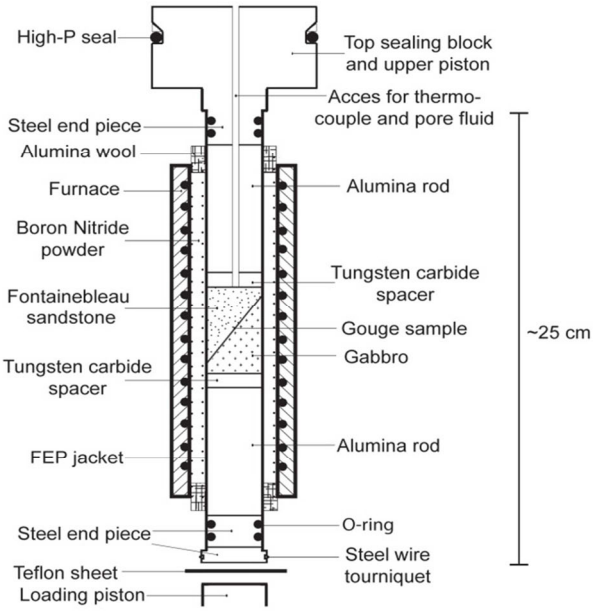

Figure 2: Experimental set up, showing the gouge sample in the centre of the sample assembly. Figure not to scale. (From Verberne et al., in press)

Verberne et al. (in press) mentioned the importance of the phenomenological rate and state dependent friction law (RSF law). These are used to macroscopically investigate the frictional properties determined and to obtain insights in the stick-slip or steady state behaviour of simulated fault gouge in laboratory and the (periodic) nature of earthquakes. It is also able to describe the transition from stable to unstable slip, as is discovered in the simulated limestone gouge (e.g. Dieterich, 1979a) and includes the rate dependence constants (a-b), which is a measure of velocity strengthening (positive (a-b) value) versus velocity weakening (negative (a-b) value) (Marone, 1998; Niemeijer and Spiers, 2007). Despite the significant error bars, Verberne et al. (in press)

showed the transition from a positive (a-b) value to a negative (a-b) value for the limestone gouge, for rising temperatures (figure 4). From formulation analysis it is determined that especially b is changing significantly, implying from the RSF law that the (thermally activated) micromechanical process behind the velocity weakening must be time or slip dependent, rather than slip velocity dependent.

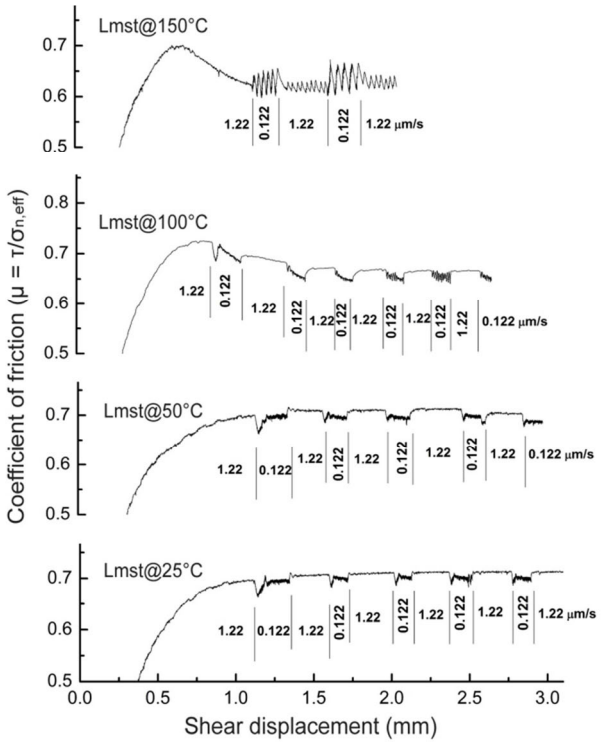

↑ *Figure 3:* Shear displacements versus coefficient of friction plots of the simulated limestone gouge sheared at 25°C-150°C. The highest temperature variant shows velocity weakening in the form of a coefficient of friction drop during the experiment. Figure modified from Verberne et al. (in press).

↓ *Figure 4:* Velocity dependence (a-b) plotted against temperature. Figures shows the change from a positive (a-b) value to a negative (a-b) value for the limestone gouge only at 150°C. Figure from Verberne et al. (2010) and for calculations, I refer to Verberne et al. (2010).

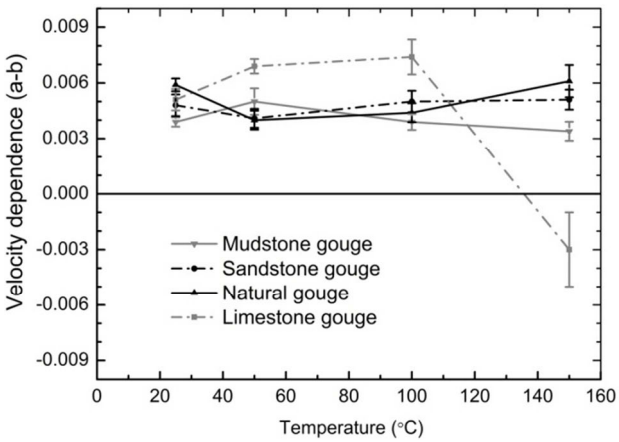

One of the main (remarking) results from the previous study is the behaviour of the limestone gouge, which shows the above mentioned transition of stable sliding (velocity strengthening) in the lower temperature regime to quasi-static oscillations (velocity weakening) with increasing temperature, with the transition at around 100°C. However, there has not been any research conducted on the microphysical reason causing the velocity weakening.

1.2. Extending the research with microstructural work: Present objectives

For several decades, many (laboratory) frictional researches have been executed on mainly phyllite rich fault gouges (e.g. Bos and Spiers, 2002; Niemeijer and Spiers, 2006 and 2007). However the (low shearing velocity) frictional behaviour of limestone gouges and the microphysical processes behind the observed velocity weakening discovered in the research by Verberne et al. (in press), has not been examined in much detail before (Billi et al., in press and references therein).

Verberne et al. (in press) proposed several candidate mechanisms which might explain the transition from velocity strengthening to velocity weakening seen in the 100°C-150°C sheared limestone gouge. These include: (a) crystal plastic deformation (such as calcite twin development), (b) subcritical or stress corrosion cracking and (c) pressure solution, each having different characteristics in the microstructure. On the basis of macroscopic research, the type of mechanism or a combination of mechanisms causing velocity weakening in the limestone gouge cannot be unequivocally identified. To investigate the process(es) involved, the limestone gouges (and less extensive the other sedimentary gouges and natural gouge) are analysed microscopically using the Leica DMRX light optical polarization microscope and the Scanning Electron Microscope, XL30S FEG. Both are located at Utrecht University. The microstructures of the gouges are analysed and any microstructural variations are carefully studied and analysed in order to find a microphysical explanation causing the velocity

weakening. The intra- and intergrain microstructures are compared at each temperature. The pre-sheared, crushed and sieved starting material is analysed and compared to seek for processes starting at lower temperatures. Also, the microstructure of the limestone gouges is roughly compared with the other sedimentary gouges to explain the continuing steady state and velocity strengthening at higher temperatures in non-limestone samples. Furthermore, the grain size distribution of the calcite grains at all temperatures (including the pre-sheared starting material) is determined, to investigate whether grain size reduction takes place at higher temperatures and at what scale. Despite the difficulties due to a very small grain size and the resolution of the microscopes, it is expected that a transition at higher temperatures is visible at both a relative low magnification and a high magnification. Whether it provides conclusive results is questionable, but any new insights in failure mechanisms might improve predicting earthquakes and their properties.

1.3. The importance of velocity weakening

Brace and Byerlee (1966) first proposed that the stick-slip instability recognized in many frictional properties studies, is analoguous to the earthquake rupture frequency (Wang, 1996). These stick-slip instabilities (unstable slip) are highly dependent on the frictional properties of the material, and they can only occur when the dynamic friction is reduced. Therefore, dynamic rock friction (strength) must play a significant role in controlling the frequency-magnitude relation of earthquakes. Velocity weakening is the phenomenon of a decrease in frictional strength (dynamic friction) with increasing sliding velocity (Niemeijer and Spiers, 2006). It is recognized as a decrease in friction after a strength peak during sliding experiments. This process of velocity weakening ranges from micro-cracks inside rocks up to tectonic faulting leading to major earthquakes all over the world (Wang, 1996). Therefore the cause of velocity weakening and the influence on the frictional properties of fault rocks has been studied a lot and will be studied in more detail in the future. This paper is part of the research, where I try to define the micromechanical processes causing velocity weakening in a simulated limestone gouge.

There are several mechanisms proposed that are able to explain velocity weakening in fault gouge more general. One of the more studied processes is the pressurization of pore fluid due to flash (or shear) heating and carbon decomposition. (Han et al, 2007a, 2007b and Sulem and Famin, 2009) This results in powder lubrication of nano-grains, a reduction of the effective mean stress and finally a reduction in the rock friction. Also the effect of phyllosilicates on velocity weakening is often studied (Niemeijer and Spiers, 2006, 2007). Continuous shearing causes phyllosilicates to become arranged parallel to the shear direction. The rearrangement of phyllosilicates results in shear localization, sliding and a reduction of shear strength. Despite continuous research, the interaction between phyllosilicates and clasts is not understood fully yet and due to the lack of significant amounts of phyllosilicates in the limestone samples, the influence of phyllosilicates on velocity weakening and material strength is only kept in mind.

1.4. Expected microstructures: hypotheses to be tested

Several microphysical mechanisms which potentially could cause velocity weakening are mentioned above. Each mechanism has its own characteristic microstructures and the identification of these microstructures may enable the mechanisms involved in the velocity weakening to be identified.

One of the proposed mechanisms is crystal plastic dislocation in the form of calcite twin development or dislocation creep. Dislocation creep is difficult to distinguish using the techniques used in this study. Transmission Electron Microscopy (TEM images) provide images of dislocations and subgrain development due to continuous dislocation creep might be found in SEM images. Twinning in calcite is recognized as thin or thick black lines or lenses (Ferril et al, 2004) within a single crystal, due to a different orientation of the twinned plane. At

temperatures encountered in this study, the main crystal plastic deformation mechanism of calcite is mechanical twinning instead of dislocation creep (Ferrill et al, 2004 and references therein). Another mechanism which might influence velocity weakening is pressure solution. Microstructural evidence for this water enhanced process is found at the grain boundaries. Matter is diffusing away from points with relative high intergranular pressure (e.g. Rutter, 1983) so at grain contacts, indentations/truncations develop whereas at the free surface, matter is precipitating. Grain contacts might become vague due to the dissolution and precipitation of the material. Also the occurrence of stylolites within compacting sediments in general gives prove for pressure solution. Stylolites are however not expected to be found here since they (generally) are a result of diagenesis. The problem arises when looking at the dissolution properties of calcite. In contrast to other materials, the dissolution rate for calcite decreases when the temperature increases (Verberne et al, in press) thus it is expected that the evidence for pressure solution decreases with temperature. A third (thermally activated) mechanism proposed is subcritical stress corrosion cracking which is often encountered in the metal industry and it is found as chemically assisted (microscopically) small cracks in the material (Dunning et al., 1994). The mode of crack propagation is in most cases mode I (tensile). The small cracks could coalescence and form a large connected crack. The effect of the chemical environment has not been studied in detail in this thesis.

Another possible mechanism is powder lubrication, which is recognized as a major process causing velocity weakening (Mizoguchi et al, 2009) and despite the low temperatures, it is possible for calcite to have such a small grain size (down to nano-scale) that powder lubrication might be possible. Finally, from the model proposed by Niemeijer (2006), different types of microstructures are expected. Despite using significant amounts of phyllosilicates, the velocity strengthening (low velocity in his model) regime shows an ordered anastomosing microstructure with phyllosilicates being the localized zones and round grains being trapped between them. The velocity weakening regime shows microstructures being less ordered, with no phyllosilicate bands and no preferred orientations. Instead of phyllosilicates, it might be possible that Riedel shear bands are the localized zones so these might be visible in the velocity strengthening regime where they could be less apparent in the velocity strengthening regime.

All these mentioned microstructures are kept in mind so that finding them and relating this to mechanical processes becomes easier.

2. Methodology

2.1. Sample preparation

Previous to this research, the samples were already experimentally sheared at the CEA laboratory in Beijing to investigate their mechanical properties, and for the pre-shearing sample preparation, I refer to Verberne et al. (in press). The experimental apparatus is described by He et al. (2006) and the detailed experimental procedure is described by Verberne et al. (in press). For the purpose of this study, the sheared cylinders used as the starting material in this research, were provided from the earlier mentioned previous study. This includes the upper (Fontainebleu sandstone) and lower (gabbro) forcing blocks, the gouge layer in between and the Fluorinated Ethylene Propylene (FEP) jacket. The cylinders are impregnated by epoxy resin (Araldite 2020) so that material is not lost during the first stages of preparation. For microstructural analysis, the samples were cut into half along the long axis of the cylinder, perpendicular to the shearing direction. The maximum amount of displacement of the simulated gouge is exposed at the surface of the sample. The newly formed surface of half the cylinder is smoothened and impregnated by epoxy resin with the same reason as above. The surface is glued on a glass plate with the same epoxy resin. Thin sections (with varying thicknesses) are sawed from one half. For each of the limestone samples, thin sections of 2000 microns thick are made. The surface is smoothed and polished carefully to get the best SEM results. Each thin section is again

impregnated with epoxy resin, to ensure that the whole sample is covered and that every structure remains in place. Reflectance light microscopy is necessary for these samples due to their thickness, but this disadvantage weights up against the reduced change of losing important microstructural features when the sections are thin.

To check whether thin sections give significant better results on the light microscope and, on the other hand, if there is no significant loss in microstructural features, the low temperature samples of the mudstone, sandstone and natural gouge are used as testing material, making the sections either 30 (mudstone gouge) or 100 (natural gouge and sandstone gouge) microns thick. Due to the very fine grain size of mainly the natural gouge (a few micrometre to maybe the nano-scale), gaps developed in the gouge band and important microstructures might be disappeared. In order to compare the sheared simulated sedimentary gouges, the starting (pre-sheared) material is also microstructurally examined. The sieved and crushed starting powder, provided by the CEA laboratory, was carefully stirred in a few millimetre thick layer of epoxy resin. The resulted suspension was emplaced in a vacuum pump for several minutes to reduce most of the bubbles. After >48 hours of drying, the samples were emplaced on a glass plate on which thin sections of ~30 microns thick are produced. On top of the samples, another layer of epoxy resin was emplaced on top of the thin sections, to reinforce the samples.

Prior to microstructural investigation, the rebound- or extension-effect of the Fluorinated Ethylene Propylene (FEP) tubing on the sample is determined. This was done in two different ways. First by simply measuring the maximum displacement of the gouge as it is at present, and then compare it with the displacement measured directly after the shearing experiment executed by Verberne et al. (in press). Another method to calculate the rebound effect, is to measure the displacement of the gouge by using light microscope photographs. The latter method provides a less erroneous result due to the higher magnification image of the gouge. The resulting rebound or extension of the sample material is taken into account when studying the microstructure of the gouges.

2.2. Light Microscopy

Since a large range of magnifications is necessary for analysis, first low magnification photographs are taken from the Leica DMRX light optical polarization microscope. Due to the thickness of the sections and the density of the grains, only reflecting light is used. The sample is rotated in the way the gabbro forcing block boundary is always horizontally orientated, with the fault gouge on top of it. The gabbro interface is taken as reference since this boundary is always relatively straight whereas the Fontainebleu sandstone forcing block boundary is more rough and variable through the sample. For simplification, the same orientation is taken for the Scanning Electron Microscope photographs. Whether the material has sheared "sinistral" or "dextral" depends on which half of the cylinder was chosen for thin section preparation. This is corrected by mirroring the picture, so that all the samples have sheared with an apparent sinistral motion. To get an overview of the sheared sample, pictures at ~5 times magnification are taken along the whole section and combined to form a sample panorama. By doing this, intra-sample differences are quickly recognized and navigation through the sample is easier when the magnification increases. The maximum (useful) magnification of the Leica (reflecting mode) is ~50 times. From light microscope photographs, interesting sample locations are chosen for further research.

2.3. Scanning Electron Microscopy

Before placing the samples in the Scanning Electron Microscope (XL30S FEG), the samples were coated by either carbon (using the Cressington 208carbon) or platinum/palladium (using the Cressington 208_{HR}), abbreviated as Pt/Pd. Carbon has the advantage that (1) it is virtual transparent under the SEM due to the low density and low layer thickness, (2) it is amorphous and (3) it has low secondary-electron emission

(Lee, 1995). On the other hand, platinum is better for high resolution pictures due to the small particle size. To increase electronic conductance and avoid electronic loading of the limestone samples at its best, a thin layer of silver was painted on each edge of the thin section.

The samples are carefully emplaced in the SEM and analysed with magnification ranging from ~125 times to ~150.000 times. Due to the polished surface of the samples, at low magnification, the Secondary Electron (SE-) detector did not show much detail. Despite the lack of chemical variations within the samples, and especially within the limestone gouges, the Back Scatter Electron (BSE-) detector was used at relatively low magnifications (up to ~25.000 times), giving clear structures. At magnifications higher than ~25.000 times, the Through the Lens Detector (TLD) was used in Ultra High Resolution mode (UHR). Secondary Electron detection resulted in high resolution, high magnification topographic photographs of the smallest portion of grains down to nano-scale size. The UHR mode is only applied on the limestone starting material and the 25°C and 150°C sheared limestone gouge samples. The latter samples are assumed to be the structural end-members thus investigating the high resolution microstructure of the intermediate limestone gouges is time consuming and unnecessary. At the high magnification scale, the porosity and the individual grains, their shapes and sizes become apparent. An increase in porosity is in many cases correlated to the velocity weakening (e.g. Niemeijer and Spiers, 2007). On the other hand, pressure solution at the grain scale contact decreases the porosity, thus investigation at this scale is important in the understanding of the micromechanical process(es) behind velocity weakening.

The photographs taken by the light microscope and the SEM are carefully analysed and compared to each other. Combining gives a magnification range from ~5 times to ~150.000 times, so structures at all possible scales are investigated.

2.4. Determining the Grain Size Distribution (GSD)

To investigate the effect of temperature on the sheared limestone gouge quantitatively, the grain size distribution is calculated. There are several ways to determine the GSD. One commonly used method is to sieve the material (e.g. Sammis et al., 1986 and Storti et al., 2003), but due to the very small grain size (<5 µm) encountered in this research, this method is not applicable (Wilson et al., 2005). Another method of determining the GSD is to use image analysing software like "imageSXM" and "ishapes" (e.g. Keulen et al., 2007 and Stunitz et al., 2010), to make, for example, the so-called "D-maps" (Heilbronner and Keulen, 2006). A third commonly used method of calculating the GSD is to use a laser particle size analyzer (e.g. Wilson et al., 2005). Such an apparatus is also used for GSD calculations on the (crushed and sieved) starting material by Verberne et al. (in press). Testing the obtained grain size results using the same method at the Utrecht University, gave approximately the same data. However, from photographs taken by the SEM and the Light Microscope, clusters of multiple grains are found and it is likely that the laser particle size analyser took the clusters as being one grain which is expected to result in multiple peaks instead of a normally distributed graph. This is further outlined in the results section (3.4.).

In multiple studies (e.g. Sammis et al., 1986, 1987; Marone and Scholtz, 1989 and Keulen et al., 2007), the fractal dimension (D) is calculated. This is the slope of the power-law distribution, when plotting the particle density against particle size in a log-log plot. The particles are self-similar when D=1.58 (in a 2D picture). Several studies have found for both natural and simulated gouge, either a log-normal or power-law particle size distribution (Marone and Scholtz, 1989).

The GSD of the limestone gouges in this research is calculated by using the linear intercept method. For the individual grains, a rough grid (with 4 vertical lines and 3 horizontal lines) is emplaced on top of SEM pictures (magnification 1500 times). Each grain boundary is indicated on top of this grid so that the grain intercept length along a grid line can be determined. This is shown in figure 5. With help of the scale bar and the number of pixels, the grain intercept size is measured. This is done for each grain along the

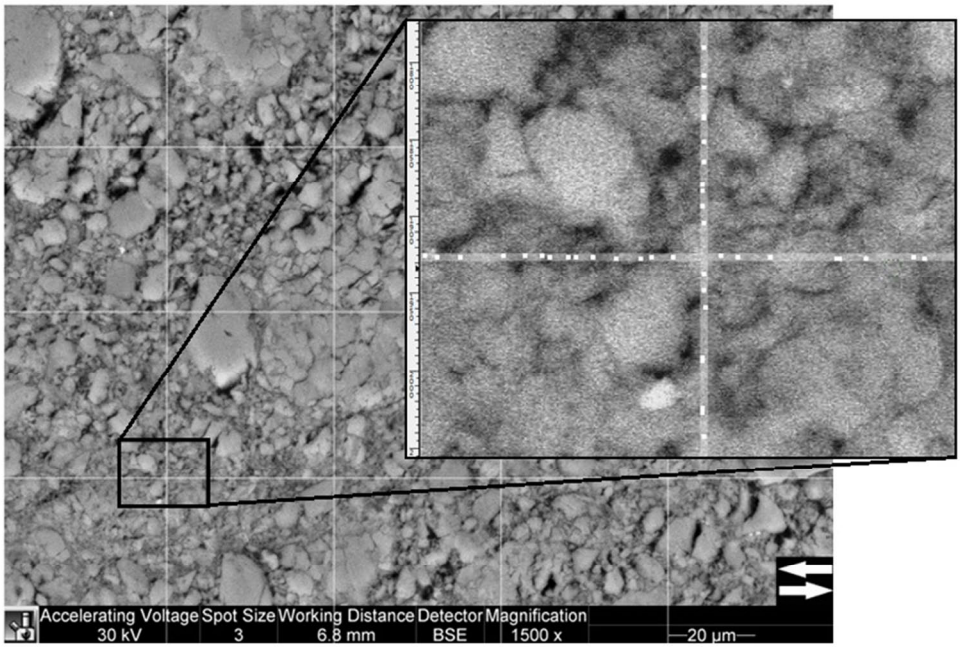

Figure 5: A schematic view on the linear intercept method as used in this report. Each grain intercept along a line is indicated by a white dot. The size of the grains is inserted in the spreadsheet application "Microsoft Excel".

horizontal and vertical lines. The grain size measured is not the maximum grain size but more an apparent grain size. The result will be essentially the same. A finer grid (9 vertical and 7 horizontal lines) is emplaced on top of the photographs used for cluster size distributions calculations (magnification 800 times) and for the starting material. This is because the grain density is decreased, where for a successful result enough grains are necessary. As mentioned above, the reason the grain clusters are calculated is that they probably behaved similar as (weak) individual grains during shearing, otherwise fractionation should have taken place already during crushing (and sieving). It is expected that the small (few µm and smaller) grains fracture less easily than large grains or in this case cluster.

All individual grain sizes were placed in different "Microsoft Excel" spreadsheets, so that the data is easily analysed in several ways: (1) The grain sizes on the horizontal and vertical grid lines could be compared to check if there is e.g. a flattening effect due to shearing. Also (2) the GSD against temperature is checked, to see if there is some grain size reduction or not. (3) The grain cluster size change with temperature is analysed and (4) a combination of individual grain size + cluster size is plotted. Due to the character of the gouge (it does not follow a power law distribution), it is (in most cases) impossible to calculate the fractal dimension of each gouge in this study, so the grain size distribution is only cumulatively determined (with cumulative number (%) on the vertical axis and grain size (µm) on the horizontal axis). However the method used here provides result sufficient enough for the purpose of this research.

2.5. Riedel Shear Orientation measurements

The orientation of each R Shear band in the sheared limestone gouge is measured with respect to the gabbro boundary. The mean orientation, standard deviation, the maximum and minimum orientation and the median are plotted in an orientation (in degrees) versus temperature (°C) diagram, as will be examined in the results and discussion sections (4.5. & 5.2.) Since the orientation of each R-shear varies quite significantly, especially in the 100°C limestone sample, only the mean orientation at the centre of the sample is considered. This is because some of the shear bands have the tendency to become flattened when approaching the driver blocks. When doing this consistent for each sample, the mean orientation of one R shear band will be sufficient to discover trends between different temperature variants. Also the number of R-Shear bands per temperature is considered since this might have a major influence on the error.

2.6. Compaction analysis

As an addition on the porosity observed in the high resolution photographs of the limestone gouge, I tried to determine the amount of compaction. For this, a combination of several light microscope photographs are used, which are fitted together on the computer. During the shearing experiment, a significant amount of gouge is extruded out of the shear band. This extruding volume must also be taken into account. The initial shear band is indicated in one colour (e.g. red) whereas the extruded material is indicated with a different colour (e.g. green). The initial thickness of the gouge layer is assumed to be equal for all the limestone samples (1 mm), and the initial length of the sample is equal to the post-shearing length without the extruded material. Knowing this, the surface/unit volume is known. The gouge layer thickness after the shearing experiment is measured from SEM pictures, by taking the mean of two ends. The "volume" of all the material is calculated by automatically counting the number of pixels comprising the squeezed material, and from the light microscope, the real surface of one pixel is known (length^2, with the length of 1 pixel known). From this, the post-shearing volume has been calculated. The initial volume – (extruded volume + post shearing band volume) gives a value of either dilation or compaction. Since the photograph is a 2D representation of the sample, the unit of extruding material and the original gouge layer is in mm^2. The compaction strain (engineering strain), based on the thinning of the gouge layer only, is calculated as followed:

$$e = \frac{\Delta l}{l_0} = \frac{l - l_0}{l_0} \quad \text{(dimensionless)} \qquad (1)$$

With l being the thickness of the gouge layer after shearing and l_0 the initial thickness. Due to the material loss from the gouge band, this compaction strain is only an apparent strain. The compaction C (%) including the extruded material is calculated as described in (2):

$$C = \left(\frac{V + V_s}{V_i}\right) \cdot 100 \quad (\%) \qquad (2)$$

Where V represents the thickness times length of the gouge layer after shearing, V_s the volume of the extruded material and V_i the initial volume of the gouge layer. If the result exceeds 100 %, the material has been dilated. Under the 100% indicates that compaction took place.

The compaction result is compared with the photograph analysis to check if the data gives similar results.

The shear strain (γ) of each sample is calculated as followed:

$$\gamma = \frac{\Delta x}{l} \quad \text{(dimensionless)} \qquad (3)$$

Where Δx is the shear displacement. The shear strain is calculated for two end-member situations: first the shear strain is calculated by using the initial thickness (l_0) of the gouge layer and second the shear strain taking the final thickness (l) of the limestone gouge is determined. This gives a maximum and minimum range of shear strain values.

Despite the ease of compaction calculations in this way, several problems emerge during the compaction calculations: (1) It is difficult to take the possibility of dilatation in the extruded volume into account, however, due to a significant stress drop at these localities, it is likely that dilatation occurs. (2) Also the loss of material of parts of the extruding volume during sample preparation and (3) the fact that photographs are a 2D representation of a 3D system. The gouge is most likely not homogeneously extruded and gouge layer thickness may vary. No corrections on the basis of these problems have been made.

3. Observations and Results

3.1. The effect of Fluorinated Ethylene Propylene (FEP) tubing on the limestone gouge

By calculating the shear displacement of the simulated limestone gouge and comparing it with the shear displacement calculated by Verberne et al. (in press), the rebound or extension due to the FEP tubing is determined. The results are shown in table 1 below.

Temperature (°C)	Shear displacement (mm) Calculated	Shear displacement (mm) Verberne et al. (in press)	Rebound / Extension
25	2.0±0.2	3.1	Rebound, FEP tubing broken
50	2.4±0.2	2.9	Rebound
100	1.8±0.1	3.0	Rebound, FEP tubing broken
150	2.3±0.2	2.0	Extension

Table 1: Shear displacement calculated and compared with displacement determined by Verberne et al. (in press) to determine the post-shearing rebound or extension due to the FEP tubing.

Please note that the estimated shear strain is not inserted in this table but implemented in table 2.

These results show significant rebound of three of the simulated limestone gouges, due to the FEP tubing. However, the highest temperature variant (150°C) shows extension. This means the shearing process most likely continued after the experiments. Despite the calculated extension, which is determined in different ways (see methodology section 2.1.), the microstructure tells different (section 2.2.). In a later section I will discuss the microstructural observations and results in more detail, but from photographs taken by both the light microscope and the Scanning Electron Microscope, it is visible that the 150°C sheared limestone gouge underwent significant rebound movement instead of continued shearing. Most of the gouge (at the right part of the sample) has been detached from the gabbro forcing block and the material still attached to the gabbro fits the topography of the released material very well if the gouge is displaced in the direction of shearing (sinistral) for approximately 500 µm. These results and observations are taken into account when studying the photographs in more detail.

3.2. Microscope observations: Limestone gouge

As will be noticed, I ordered the limestone microscope observations by temperature. The figures are emplaced at the end of this results section. In this report, I will talk about "left" and "right". These are the real (non-mirrored) left and right part of the gouge band, with the gabbro forcing block horizontally below the simulated gouge. Each limestone sample (25°C, 50°C, 100°C and 150°C) is emplaced under the Leica DMRX light optical polarization microscope and the Scanning Electron Microscope (SEM), XL30S FEG. Recall from the methods section (2.3.) that the SEM-observations, as summed below, can be divided into two parts: (1) The part where photographs are taken by using the BSE detector, with magnifications ranging from 100 times up to 25.000 times and (2) the part where photographs are taken under ultra-high resolution mode (UHR), using the TLD (Through the Lens Detector with SE imaging). For this mode, the magnification ranges from 25.000 times up to 200.000 times. This second UHR part is only applied on the two end-member temperature samples: 25°C and 150°C and the starting material.

3.2.1. Sample deformed at 25°C

Light Microscope (figure 6): The 25°C deformed gouge shows significant differences between the left and right part. First of all, the photographs are darker at the right part, possibly inhomogeneous appearance of the epoxy resin. Due to these dark areas, the detailed microstructure is difficult to investigate. Another left versus right difference is the microstructure. In figure 6 it is visible that at the left (light) part of the sample, a well-developed microstructure is lacking whereas on the right (dark) part, microstructures are clearly available, even despite the dark nature of the pictures. The inhomogeneously distributed microstructure might be related to the limestone gouge – Fontainebleu sandstone contact, which is rough at the right part of the sample and smooth at the left part. At the rough interface, gouge has been sheared within the pores of the sandstone. Within the more evolved right part, en-echelon Riedel shear bands developed during shearing. These relatively thin R shear bands (being a line on the light microscope photographs) make an angle with respect to the gabbro interface of ~23°. One disadvantage of the

use of reflectance light microscopy is that the (internal) crystal structure is not outlined as well as with the cross polarized light (XPL) settings of the transmitted light mode. Despite this, higher (~20 times) magnification light microscope photographs of the limestone samples in general shows a significant amount of calcite e-twinning (figure 7, please note that this picture is from the 50°C deformed limestone gouge). These relatively thick (low density) twins are also recognized in the starting material, which has been observed under the transmitted light microscope. The thick twins in the starting material and in this sample are more lense shaped than thin twins. Due to these different approaches, comparison between the starting material and the sheared material, and especially the number of twins, is difficult.

Another striking observation (not well visible in figure 6) is the polycrystalline nature of the calcite grains, surrounded by a so-called matrix. These relatively large clusters look patchy under the optical microscope (maximum size equals the 200 mesh sieve (75 µm)) and are homogeneously distributed over the sample. This structure is inherited from the starting material and it apparently was only minor affected by the shearing experiment. At both ends and at all temperatures, material has been extruded from (originally 1 mm thick) gouge band, and form bulges with many cracks and an unorganized structure. The microstructure of these bulges is not further investigated, since this is completely destroyed and does not represent the microstructure caused by shearing anymore.

SEM (figures 8-15): At low magnifications, the dilatational gaps which are not visible using the optical microscope are visible very well. These are developed at especially the lower part of the sample, near the gabbro forcing block and at both sides (figure 9). The amount of post-shearing dilatation is, when using the gaps only, approximately equal on both sides. This dilatation is at the left part of the sample (figure 8), mostly accommodated at the forcing blocks interfaces whereas at the right part, the dilatation is more accommodated within Riedel shear bands (figure 10), which are more common in this part. Assuming the locations of post-shear cracking/dilation is related to locally weaker material, this might be related to grain size reduction (of relative large grains) occurring in Riedel shear bands (Y and R) and observed in the photographs. Riedel shear bands are well visible in SEM photographs (figures 9-12), showing the thin (max. 20 µm) and slightly braiding nature of the R bands. These bands destructed larger grains and polycrystalline groups causing straight shear band – grain interfaces. From the study conducted here, I was unable to determine the displacement along an individual shear band. Tracing transected grains proved to be hard since these are completely destroyed. Due to the homogeneity of the limestone gouge (~95% calcite), the search for scattered grain residue is impossible. This material disappears in the mass, becoming part of the matrix (no figure). Y shearing at the gabbro (lower) part of the sample is well visible, showing an (apparent) grain size reduction, not containing large grains. The thickness of this band is approximately 15 µm. Despite the BSE detector used (instead of SE), e-twinning in calcite grains is rare but visible (figure 11). Visible twinned grains consist of approximately 1% of the total number of grains and often occur in the larger grains. However, also individual grains within a polycrystalline cluster, which have a small size (~5 µm), appears to be twinned in several cases (figure 11). These twins are most likely inherited from the starting material. The intragranular fracturing (as mentioned in the optical microscope part) is very well visible under the SEM (figure 9 & 11). This fracturing appears to be inhomogeneously distributed.

At high magnification (figures 13-15), several pictures within the matrix (figure 13) (where no Riedel shear bands or any other type of shearing induced microstructure is observed), and in R and Y shear bands have been taken (respectively figure 13 and 14). The microstructures of these three locations are compared with each other. At magnifications 50.000 times and higher, the individual grains are visible. In general, these grains are round, having a minimum size of 50 nm.

Also the relative high porosity of the material is visible at this magnification. No exact porosity value is calculated due to the 3D view in the photographs. However, there are some remarkable differences within the lime@25 sample: The photographs taken in the so-called matrix show the individual grains packed together. Distinguishing between the grains is possible in most cases, but loose (non-grouped) grains are not recognized (figure 13). The photographs show some kind of layering of the groups. The high magnification R-shear photographs also show the individual grains, being grouped together. However, the individual grains appear to be less recognizable in some groups (figure 14). The grains might be sintered together, forming elongated clusters instead of the more oval shape clusters. Porosity is approximately equal to the matrix. The Y-shear shows even a more different picture. The round grains are not grouped or sintered and are very well recognizable. Porosity might be even higher compared to the matrix and R-shear photographs, and no elongated multigrain shapes have been developed (figure 15). There are no small fragments; each grain is approximately equally sized, having a mean size approximately equal to the matrix grain size, with the difference that the matrix grain size is more variable.

3.2.2. Sample deformed at 50°C

Light Microscope (figure 16): The 50°C deformed limestone shows also significant differences between left and right. Again, the left side shows less developed structures when compared to the right side. This left part also has a sharper sandstone – gouge interface. As visible in figure 16, the R shear band density (in the right part of the sample) is higher compared to the 25°C deformed sample. These, relative thin but presumably dense Riedel bands have a more braided pattern and seem to deflect at the gabbro and sandstone boundaries to form eventually Y shear bands parallel and close to the driver interface(s). In the 50°C sample, such Y-shearing is well developed at both the interfaces, locally forming fine grained bands and regions parallel to the shearing direction. There is no direct or indirect evidence on the displacement distance along such shear bands. Note that initially, the samples were sectioned on the other half of the cylinder, causing mirrored images compared to the 25°C. By mirroring the picture, the effects of this sampling is removed, giving all the (limestone) samples a sinistral sense of shear. The relative large grains (>10 µm) shows some mode I type of intragranular cracking with cracks in the direction of the maximum stress. Within the cracks, evidence for post-shearing dilation is found in the form of epoxy resin filled holes. The gaps between the two parts of originally one grain are recognized as broad dark lines. Also stepping in R shear bands and the dilatation of these steps is evidence for this gouge band dilatation, however this is poorly visible in optical microscope photographs. Furthermore, the polycrystalline “grains” are still very common, not showing any observational changes at this scale. These polycrystalline grains are absent within Riedel shear bands. The density of calcite twins is, based on qualitative observations, approximately equal to the lower temperature sample (Figure 7)

SEM (figures 17-19): A pronounced R-shear band at the right part of the sample provides confirmation that rebound due to the FEP jacket took place, at least in this sample (figure 18). This Riedel shear is stepped, and by moving the top and bottom part of the Riedel shear in opposite shearing direction, a gap at the step develops. This gap measures ~150 µm along the Riedel shear slip direction. Other R-shear bands show the same but less developed structure (figure 19), and also at higher magnifications, equal type of gaps developed (size ~5 µm). The R-shears are very abundant, do not braid as much and grains are cut off by those Riedel shear bands. Y shearing at the Fontainebleu sandstone (upper) part is clearly visible. During shearing, the material above this Y-shear band does not appears to be affected. It was locked during shearing and the movement occurred along the Y shear in this part. Evidence for Y-shearing at the gabbro side is less obvious in this sample. Larger grains (or polycrystalline groups) are apparent near the gabbro-gouge interface. En-echelon faulting within one grain or polycrystalline

cluster is more common (figure 17). Twinned calcite grains are not recognized in this sample and the polycrystalline nature of the larger grain (groups) is less visible. The possible reason for that is indicated in the discussion section (4.3.).

3.2.3. Sample deformed at 100°C

Light Microscope (figure 20): Within the 100°C limestone sample, there is again a large difference between left and right, with the relative large middle part being poorly visible. At this zone, the photographs show only a dark area and microstructures are not observable. The part where microstructures are not developed in this sample is relatively large with the consequence that there is at the other side of the sample a relative small, microstructurally well developed area. How microstructures vary from left to is, based on the optical microscope photographs, unknown. The sample (figure 20) shows (again) at the right part of the sample, a large amount of R shear bands. These bands are more variable in orientation compared to the 25°C and 50°C limestone samples, and they seem to braid more. Y shear bands along the sandstone and gabbro boundary have been developed, although less obvious as in the 50°C sample. On the other hand, horizontal (Y) shear bands are found within the gouge band, as a consequence of the braided nature. Intragranular cracking seems to be equally common in this sample compared to the lower temperature variant, whereas on the other hand, calcite twinning appears to be more common. Groups of twinned grains in especially the well-developed zone are found, with most of the relative large grains being twinned. Please note again that based on these photographs, it is difficult or even impossible to make a distinction between the post-shearing developed twins and the twins already available in the starting material. Multiple studies have been focusing on the several properties of calcite e-twinning with a special interest in the thickness and density related to temperature and pressure (e.g. Rowe and Rutter (1990); Burkhard (1993) and Ferril et al. (2004)). In these samples, calcite twin density is relatively low with the twins being relatively thick. How thick they are is undeterminable by the optical microscope due to the low magnification but will be better outlined when studying the SEM pictures. The polycrystalline nature of the larger grains/clusters has not been changed in a significant way and any preferred orientation of both the larger grains and the smaller grains has not been found quantitatively.

SEM (figures 21-22): This sample does not vary very much from the 50°C. Most of the features mentioned above are only developed further. The intragranular cracking is more common (figure 21) and the Riedel shear bands are more abundant. However, these Riedel shear bands appear to have a more braided structure and might be a little bit wider. There is in this case, no clear evidence for Y-shearing near the Fontainebleu sandstone interface, but for this temperature variant, clear Y-shearing at the gabbro interface has developed. This "switch" of Y-shear location is likely coincidence. These shear bands probably generated randomly, lowering the shear stress so that Y-shear development elsewhere is less likely. The larger, mostly fractured grains appear to have a slight preferred orientation, with the long axis in the direction of maximum stress. This sample could not be studied completely since the centre part of the gouge band charged in the SEM, giving an over-exposed picture, despite double coating and silver painting the sample. As mentioned above, no high resolution pictures are taken from this sample.

3.2.4. Sample deformed at 150°C

Light Microscope (figure 23): Since the velocity weakening effect of the limestone has been found in this higher temperature sample, a change in microstructure is expected. Based on the optical microscope images, there seems to be little difference between left and right. However, the area which is dark is very large (~70%) and microstructures are difficult to analyse. The sandstone boundary is throughout the sample relatively rough and R shear bands are relatively uncommon compared to the lower temperature limestone samples. The shear bands which are

apparent are less developed seems to be broader and do not braid or deflect. Evidence for Y shearing is not convincing. Despite the dark nature of the picture, individual grains are still visible: the polycrystalline "grains" are still recognizable though less obvious, maybe due to a decrease in size. They seem to be more fractured although this could be the appearance due to the dark photograph. Also the amount of twinned calcite grains seems to be larger than the lower temperature variants, with the intragrain twin density being higher. At the right part, a large "thrust-fault" cuts the whole sample, influencing the structures on the right. A large gap filled with epoxy resin has been found at the place where originally the "hanging wall" was located. Also the thickness of the simulated gouge is significantly thinner at the right part. This despite the fact that the whole gouge layer is very much thinner (~500 µm) compared to the starting situation of 1 mm thickness. This is outlined a bit more in a later stadium. Overall, throughout the sample, the microstructure appears to be more chaotic. There is no preferred orientation of the grains, the shear bands are not as narrow when comparing with the lower temperature limestone samples and the larger grains look more fractured. This fracturing is not only in the σ_1 direction, but it appears to be more random. This leads to a possible grain size reduction of especially the larger grains or polycrystalline clusters. However, on the base of these photographs, this cannot be quantified and it will be outlined more in a later stage.

SEM (figures 24-31): For this sample, also UHR photographs have been taken. At intermediate magnification, it is clear this limestone gouge differs remarkably from the lower temperature variants (as mentioned before). As mentioned in section 3.2.4., the right end of the sample has been destroyed by a post-shearing rebound "thrusting" event, which is even better visible by SEM pictures (no figure). The Riedel shear bands, which developed at lower temperature, are much sharper, less thicker and better visible than those developed in this sample (figures 24-26). Distinguishing between R-shear bands and damaged material is difficult. The large grains are more fractured, and grain size reduction of especially the large polycrystalline groups and grains appears to be significant. Fracturing of these groups occurs mainly along the individual grains, so that the broken grains become one with the finer grained matrix. But also the angularity (as studied by Storti et al., 2007) of the large grains appear to increase. Bear in mind that a more detailed (quantitative) analysis on the grain size distribution has been executed on the limestone samples. The result of this is indicated later. At the right side of the sample, there is no clear indication for significant Y-shearing (figure 24) thus (almost) all of the shearing motion must have been accommodated over the whole sample. At magnifications of ~2000 times, it is visible that the amount of twinned grains increased dramatically (figures 26-28). This is especially valid for the large grains. In some cases, the twinning is so strong that the grain appears to be broken (along the twin planes) into several twinned pieces (figures 27-28). Both thick (mentioned earlier) as well as thin twins are present. These thin twins are relative straight and abundant. Some of the large grains are (still) angular and appear to be unaffected, but evidence for chipping, a late stage process of grain size reduction (e.g. Heilbronner and Keulen, 2006 and Billi et al., in press) is found in the form of angular remnants close to the angular grains. The grains (neither the large nor the small) do not show any preferred orientation. Also from SEM observations, the whole structure looks much more chaotic compared to before.

It is expected that at high magnification (UHR mode), the microstructure also differs from the 25°C variant. The grains form groups with some of the grain groups have a more elongated shape compared to the lower temperature variant (figures 29-31). These elongated groups formed bridge-like structures with relative large pores in between. These bridge-like structures are also recognized in the 25°C sample, within R-shear bands. Evidence for actually seeing individual grains is found in the rare case that grains appear to be faceted in the way calcite is expected to be present (figure 31). The porosity appears to be

higher than the porosity of the low temperature variant. Also, some of the grains appear to be sintered to each other more than at 25°C. Despite this difference, the lower temperature structure is locally still recognized. Individual grains are visible and the grain size does not seem to be decreased. Also the more round/oval grain cluster structure is still apparent at random locations. The high magnification R-shear photographs (figure 30) show a more evolved structure, with an apparent higher porosity and more (evolved) elongated structures, where the individual grains are still visible. These elongated (bridge) structures are finer and make up most of the microstructure. Round/oval grain clusters (such as in the low temperature variant) are more rare. Sintering of the grains appears to be approximately equal compared to the matrix and the grain size seems to be slightly reduced. The grain shape does not change (significantly). Also high magnification photographs of a Y shear along the gabbro driver block has been taken (figure 31). This Y shear is less developed than the Y shear photographed in the 25°C sample, but despite this, the structure differs somewhat from the matrix and R shear band. The bridging structure is again finer but the elongated shapes appear to be shorter relative to the R shear band structures. It resembles the low temperature variant in the way that individual grains are relative well recognized, with the difference that elongated structures are still apparent. This might have something to do with the less evolved nature of the Y shear instead of temperature differences only.

Please note that the surface effect might have a major influence in interpreting these photographs. Figure 30 and 31 show a part of a larger (few µm) grains (respectively the upper and the lower right part of the photograph). The surface of these individual large grains are relatively rough with asperities having the same size as some supposed individual grains. Despite the lack of large grains in the low (25°C) temperature sample, the surface effect could also become a problem in that sample.

3.2.5. Limestone starting material

Light Microscope and SEM (figures 32-34): Twinning is recognized in the starting material when using the light microscope, however it is very difficult to distinguish twinned grains from non-twinned grains under the SEM. In general, the grains and polycrystalline clusters have a rough shape and possible twinned grains are more angular (figure 32). There is not a so-called matrix, and to compare with the high resolution matrix photographs of the sheared gouge therefore is very difficult. The resulting photograph depends highly chosen location. The area's where either material is fallen out or epoxy resin has not penetrated appears to be the best for high magnification comparison (figures 33-34). These places show very well the individual grains which are often round (depending on the location), forming elongated shapes when grouped together. The elongated groups do not "bridge" and act more as fibres and individual grains. Within polycrystalline groups, the individual round grains are locally visible, appearing to be equal to the material found in the sheared gouge. The smoothened surface of a polycrystalline cluster shows a mud-crack like pattern.

3.3. Microscope observations: Other gouges

The other sedimentary gouges and the natural gouge are not extensively studied, however the presence of some microstructures, or even more important, the lack of other microstructures could be of importance when studying the limestone gouge. Therefore a summary of the observations of the other gouges is shown below:

3.3.1. Samples deformed at 25°C and 150°C

Light Microscope observations: The differences between the low and high temperature gouges are minimal. In both the simulated mudstone gouges and the natural gouges, no Riedel shear bands developed and in the sandstone, Riedel shear development was only very minor. These shear bands did not evolve with higher temperatures. This differs significantly from the simulated limestone gouge, which shows in any case major R-shear development. In these limestone gouges,

Riedel shear bands make up the rough microstructure whereas the other gouges show a more homogeneous and structureless microstructure.

The simulated mudstone gouge and sandstone gouge resembles each other. Both show homogeneously distributed larger grains (respectively ~75 µm and ~50 µm, in correspondence with Verberne et al., in press) surrounded by a "matrix" of finer grains. On the other hand, the simulated gouge appears different from previous mentioned gouges. Due to the different sample preparation by Verberne et al. (in press) and the nature of occurrence, the variety in grain type, grain size and grain shape is large. It is impossible to distinguish between the so-called matrix and grains. This structure does not seem to change with temperature. The large grain size appears to be equal and the material remains homogeneously distributed.

In general, thicknesses of the low temperature samples vary significantly (especially the sandstone gouge thickness), whereas the Fontainebleu sandstone driver block interface does not change within the sample (as much as in the limestone gouge sample). The thicknesses of the higher temperature variants are more stable. This is probably not an important difference.
Furthermore, any other structures produced during the shearing experiment are at least not visible using the Leica optical microscope only. Grain contacts, detailed grain shapes and intra-grain structures cannot be studied at the magnifications reached.

SEM Observations: From SEM pictures it is clear that the sandstone resembles the limestone the most. It shows some R-shear development, a clear Y-shear at the sandstone boundary and a smaller Y-shear at the gabbro side of the sample. The R-shear bands are broader and less common as in the limestone. The sandstone also has larger grains floating in a finer grained matrix. The large grains are relative angular compared to the limestone and the matrix consists of mostly fibrous and some angular grains. The chemical diversity (as visible by the BSE-detector) between and within the grain is larger. Post-shearing dilatation appears to be less. The material was not released from the driver blocks.

The more homogeneous mudstone gouge has larger (maximum) grains compared to the sand- and limestone, with the grain-matrix ratio being larger. The compositional differences are also higher compared to the limestone gouge, with the matrix being fibrous (rich in phyllosilicates) as well. The SEM photographs do not show (clear) Riedel shear bands within the sandstone, which is in correspondence with the optical microscope observations. A part of the larger mudstone grains have gaps in and at the edges of the grains. Whether this is due to shearing, inherited from the starting material or due to sample preparation cannot be said.

Analysing the natural gouge is a bit more difficult due to the quality of the sample. However, it can be observed that the diversity (both the grain structure as well as the compositional differences) within the natural gouge is large. The matrix is very fine and fibrous, showing a flow-like pattern. The smallest grain size and porosity cannot be observed by the magnification used here, but it might be approximately similar as the simulated limestone (as indicated by Verberne et al., in press). There have no Riedel shear bands been developed and, despite the heterogeneity of the grains, the material appears to be distributed quite homogeneously.

Taking all the observations, the non-limestone gouges do not show (as much) Riedel shear bands (neither R nor Y shear bands), thus shearing must have been accommodated over the whole sample and is not localized. Also the differences between left and right (as seen in the limestone gouges) are not observed in the mudstone, sandstone and natural gouge. From high magnification photographs, it is observed in the limestone that the matrix does not have significant amounts of fibrous minerals whereas the other three types of gouges all have fibrous constituents in the matrix.

3.4. Grain Size Distribution (GSD) analysis

In this section, the grain size distribution of the limestone gouge (only) is quantitatively

determined. The reason for choosing the linear intercept method (figure 5) is described in the methodology section (2.4.). The figures I refer to are also located at the end of the results section.

The first part of GSD calculations, is the determination of the distribution of each grain encountered in photographs at the magnification of 1500. This includes the individual grains located in polycrystalline clusters. The 25°C and 150°C samples are taken to be the so-called end-members samples, and therefore approximately double the grains are calculated. The number (#) of grains used to construct figure 35 and figure 36, is 863 + 460 + 367 + 857 for respectively the 25°C, 50°C, 100°C and 150°C lines. In figure 36 you can see the results from the GSD calculations for each temperature and all grains. From the graph you can see the grain size is very small (mean ~2 µm) and approximately equal for each temperature. The maximum grain size lying around 5 µm with some exceptions reaching the size of 10 µm. with respect to the grain size, not much changes when varying the temperature. A slight decrease in grain size might be visible for the highest two temperature variants (100°C and 150°C). Please note that the magnification is only 1500 times and that the grains below 0.5 µm (500 nm) are not visible at this scale. From the results mentioned in the SEM observation section 3.2., it is observed that a significant amount of grains have sizes below the observable grain size and therefore it is likely that nano-grain sized clusters are taken as individual grains.

One advantage of a superimposed grid as used in this study, is that also the possible differences within a sample can be determined. Due to shearing, some preferred orientation might be expected, leading to for example flattening of the grains. This flattening should be observable when comparing the horizontal grid data with the vertical. If flattening indeed appears to be the case, the grain intercept length along the vertical grid lines is smaller compared to the horizontal grid lines. This has been done for the limestone gouge grains (including the grains in the polycrystalline material). From the results obtained (figure 35), you can see there is a small difference between horizontal and vertical data. At higher temperatures there seems to be a small preference for the grains to be larger in vertical direction, thus perpendicular to the shear direction. The result of the horizontal data versus vertical data is shown in figure 35. This figure includes all the limestone data as used before. Vertical data is marked by the colour blue and horizontal data is green. The more dashed a line is, the lower the temperature.

The Grain Size Distribution of the limestone gouges without the polycrystalline groups/clusters is also calculated since these clusters most likely act as individual grains. They are also apparent in the starting material and appear to be only minimal affected by the grinding, sieving and shearing processes it underwent. The result of the GSD calculations without the polycrystalline clusters and their constituent grains is shown in figure 37. The graph is based on 619 + 393 + 281 + 503 grains for respectively the 25°C, 50°C, 100°C and 150°C data. From this graph, it is visible that the grains are smaller compared to the GSD of figure 36. This is because the grains within the polycrystalline clusters are relative large compared to the grain size of the matrix. By excluding the grains within the polycrystalline material, only the relative small sized matrix remains. The grain size of the matrix does not seem decrease with higher temperature. Please note that the starting material is also included in the graph (having the lightest colour). The grain size of the starting material approximately equals the size of the highest (150°C) temperature variant. So the grain size of the matrix is apparently not affected by the shearing experiment.

Since the matrix does not show any decrease (or increase) in grain size, the polycrystalline clusters are taken to determine the Grain Size Distribution. These relative large structures are most likely more affected by shearing due to their size, and if grain size reduction takes place, it is expected to be found in the polycrystalline clusters. These clusters have also the grain boundaries as distributed lines of weakness (as found in the SEM photographs, where fracturing occurs at these boundaries). As mentioned before,

because of the size and the occurrence of these clusters, the GSD is calculated with a finer grid as before and at a lower magnification (800 times). The result of the GSD of the polycrystalline clusters is presented in figure 38. This graph is based on 288 + 220 + 300 + 369 “grains”. Figure 35 is a statistic graph based on the same data and shows the mean grain size for each temperature, together with the median and standard deviation. In both figures, a clear decrease in grain size with temperature is found. Here the starting material is not included, but the trend is clear. The mean grain size shifts from 15 µm for the 25°C deformed limestone towards ~10.5 µm for the 150°C deformed limestone gouge. At the lowest grain size measured (5 µm, in this graph), 28% of the grains deformed at 150°C have a smaller size whereas this value is 10% for the grains deformed at 25°C. This reduction is also noted by only observing the pictures and thus lies in line with the expectations. The cluster size reduction leads to an increase volume percentage of the fine grained matrix, which might be important for further interpretation.

3.5. R-Shear band orientation analysis

In the limestone gouge, Riedel shear bands are very common. As mentioned earlier, it is impossible to determine the displacement along an individual shear band (Y- or R-shear band). To quantify some properties of R-shear bands, the (mean) orientation of these bands with respect to the Y-shear band is calculated. The reason behind this calculation is based on the accommodation problems evolving when R-shear bands develop. The results from the orientation measurements are shown in figure 40. This graph shows the mean Riedel shear orientation, the standard deviation, minimum and maximum orientation and the median, all against temperature. Here you can see the mean R-shear orientation slightly decreases from 25°C to 50°C, from 23° to 18°. At higher temperatures, the orientations of the shear bands remain approximately equal. The maximum orientation changes from 30° to 24° with increasing temperature, with on the other hand the minimum orientation increasing (slightly) with orientation after a slight decrease from 25°C to 50°C of ~5°. The standard deviation remains approximately equal. Please note that the number of R-shear bands vary for each temperature: for the 25°C sample, 21 R-shear band orientations have been calculated, for 50°C sample 70 bands, for 100°C sample 35 shear bands and for 150°C only 11 shear bands. This is number is highly dependent on the clarity of the shear bands and of course the number of bands present in the sample. For example, the 150°C sample has very broad and difficult to recognize shear bands thus little R-shears could be measured.

3.6. Compaction analysis from surface calculations

I already observed the porosity of the simulated limestone gouge and as an addition on the qualitative analysis, the compaction / dilatation of the material is calculated on the basis of 2D pictures. From the equations (1)-(3) provided in the methodology section (2.6), I calculated the compaction strain (equation (1)), the compaction including the volume of the extrude volume (equation (2)), and the two end-member variants of the shear strain (equation (3)). The results are visible in table 2:

Table 2: Compaction analysis on the simulated limestone gouge. Calculations are based on equations (1) – (3) mentioned in the methods section. The X means that this value could not be measured. This is due to material loss during sample preparation. The results show an increase in compaction strain and an increase in shear strain (taking l).

Temperature (°C)	**Compaction Strain e**	**Compaction (%)**	**Shear Strain γ (taking l)**	**Shear Strain γ (taking l_0)**
25.0	-0,2	89,4	3,9	3,12
50.0	-0,2	91	3,64	2,9
100	-0,29	83,1	4,24	3,01
150	-0,57	X	4,62	2,01

From the table above, it can be seen that all the limestone samples show compaction. However, the compaction of the highest temperature variant (150°C) could not be measured, due to the disappearance of extruded material probably during sample preparation. This extruded material could not be measured thus the compaction was not determined. However, the thickness of the simulated limestone gouge is approximately half the original thickness whereas the poured material volume on the side which was still apparent was relative low. This can also be observed in the compaction strain results. The compaction strain value for the 150°C sample is approximately two times higher compared to the lower temperature variants. The shear strain calculated from the thickness of the layer and the shear displacement shows an increase in shear strain when taking the post-shearing thickness and no relation when taking the initial thickness. This last value is one to one related thus affected by the shearing experiment.

When comparing it with the observations made by investigating SEM photographs, the result is remarkably different. The material appears to be dilated slightly from the photographs, whereas the compaction analysis executed here shows compaction, which is related to a lowering in porosity instead of an increase.

3.7. Summary of results

When a study delivers a large amount of data, it is important to filter out important trends and main results. This is also the case for the study conducted here and trends and main observations will be summed below:

- *Riedel shear bands:* One of the main trends found within the limestone gouge is the number of R-shear bands which increase with higher temperature with the highest temperature variant being an important exception. The 150°C limestone sample shows less R shear bands which have a broader and less developed signature. The orientation of the R shear bands appears to change with temperature, with the highest temperature R shear bands having the smallest angle with respect to the shearing direction.
- *Plastic deformation:* Calcite twinning appears to increase with temperature, although it is important to note that twins are already present in the starting material.

GSD: Grain size reduction of the large calcite grains / clusters occurs and this (hypothetically) causes an increase in the so-called matrix. The smallest grain size in the matrix reaches approximately 50 nm and appears to be equal for all limestone variants.

- *Compaction*: The final thickness of the 150°C gouge layer is remarkable because it is approximately half of the initial thickness. However, the porosity appears to be equal or even higher compared to the lower temperature variants and further evidence for compaction has not been found.
- *Pressure solution:* Evidence for an increase (or decrease) in intergranular pressure solution is not strong. However, an increase in so-called sintering of the grains for the high temperature limestone gouge might imply that pressure solution increased with temperature. This possibly formed the bridge-like shapes developed at the grain scale.
- *Other gouges*: The similarities between the limestone gouge, which showed the velocity weakening, and the other gouges, which showed only velocity strengthening behaviour, are small. No (or very little) R-shear bands developed, the gouge layer has not thinned extremely, there is no clear fractioning (grain size reduction) and also the matrix of each sample differs significantly from the limestone matrix. On the other hand, the properties of the other gouges which are not shared with the limestone gouges are often shared with the other non-limestone samples.

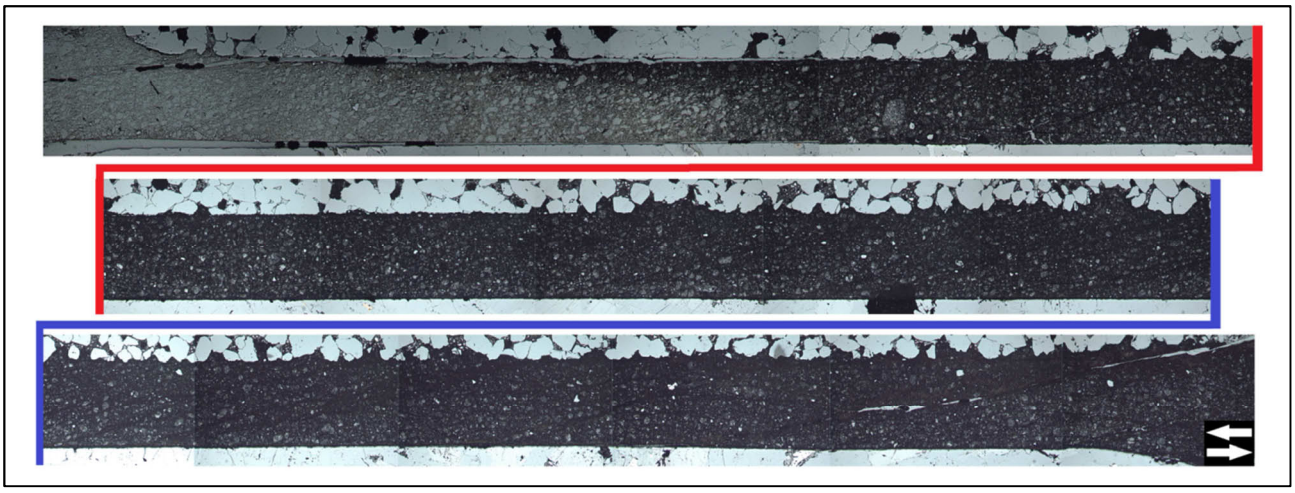

Figure 6: Panoramic photograph made by the optical microscope of the 25°C deformed limestone gouge (sinistral). This gouge band is divided in three parts, with the red and blue lines fitting the ends of a piece. The roughness of the sandstone and the darkness of the picture at one end is clearly visible. Riedel shear bands are common at the right (lower) part. The whole gouge layer length, for all the limestone samples, is ~330 mm.

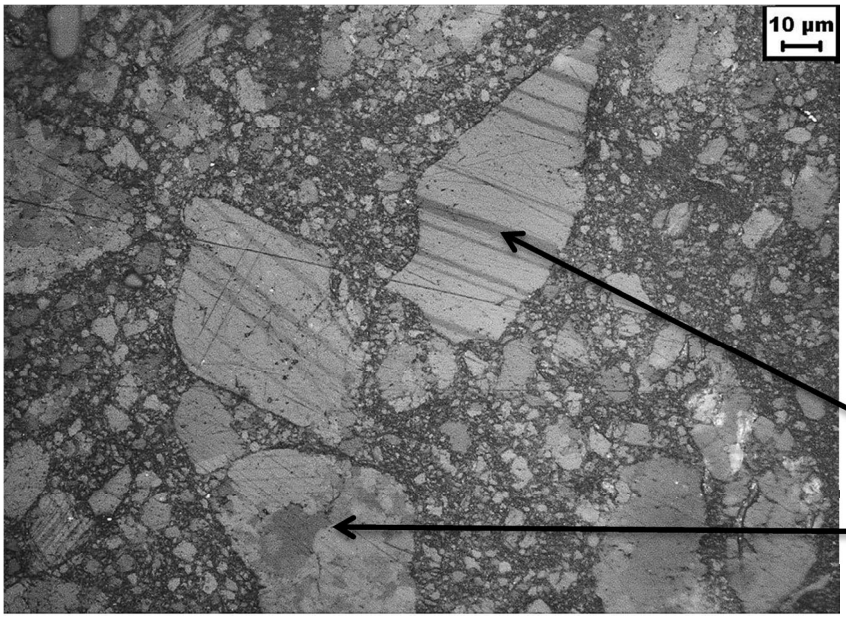

Figure 7: Light optical microscope photograph of the 50°C deformed limestone gouge, taken at ~50 times magnification. The photo clearly shows the twinning in some calcite grains and the patchy structure in other calcite grains. The patchy polycrystalline clusters are in general more round than the twinned grains.

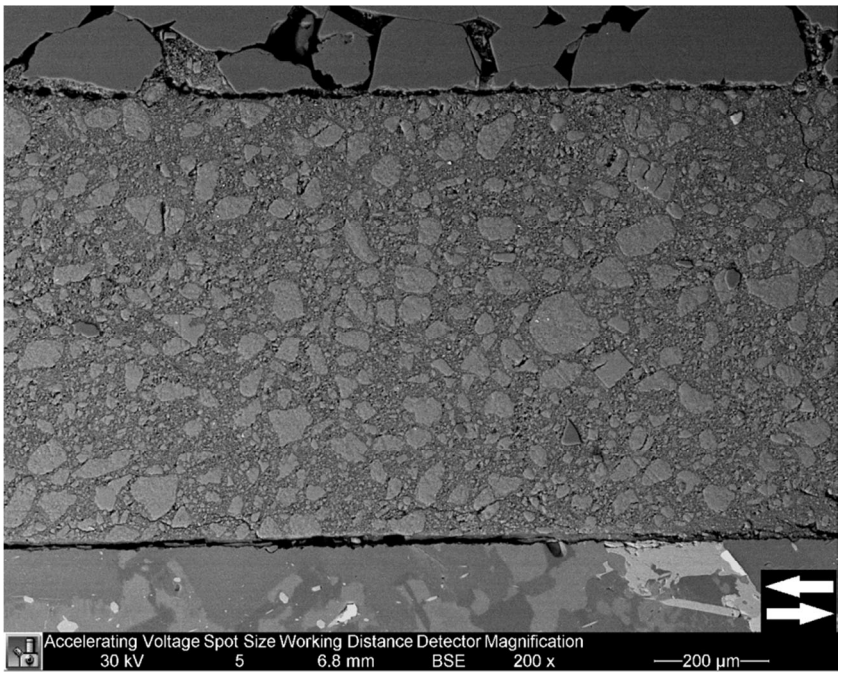

Figure 8: SEM photograph of the 25°C deformed limestone gouge. This picture shows the structureless nature of the left part of the gouge. No R or Y shears have been found and the sandstone boundary is sharp. Some grains have been broken, but no further structures are found.

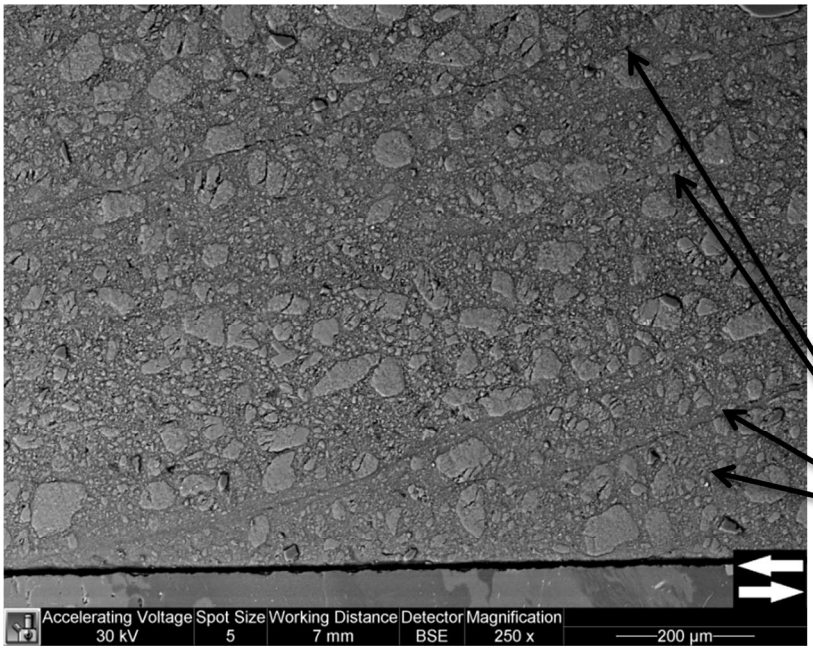

Figure 9: SEM photograph of the 25°C deformed limestone gouge. This photograph is taken more to the right, where R-shear bands are common. These bands have a thin and straight nature. Deflection is little and no Y shear band has been developed at this place. Somewhat more grains appear to be intergranularly fractured at this location.

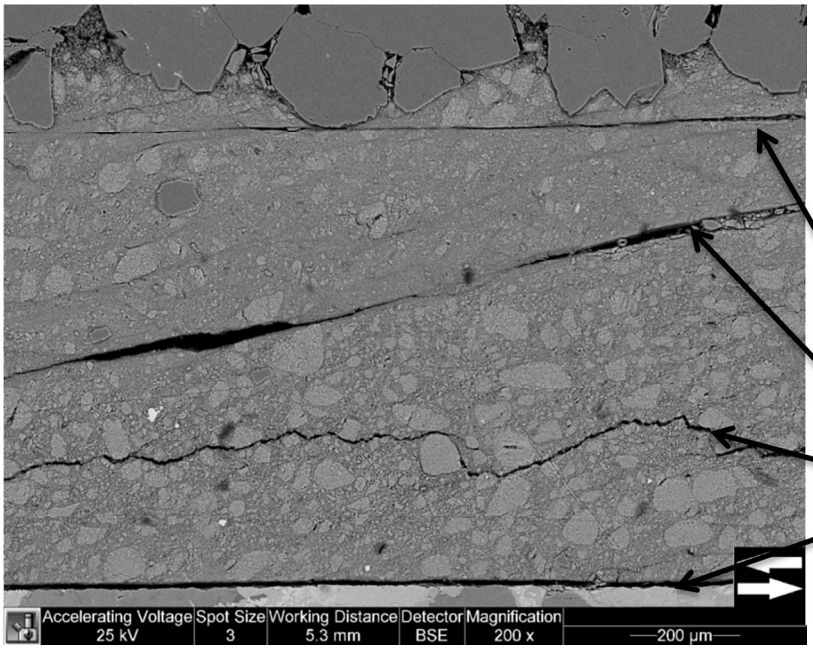

Figure 10: SEM photograph of the 25°C deformed limestone gouge at the right zone of the sample. Many R shears have developed and at the sandstone driver block, a sharp Y shear has developed. This picture shows the gaps developed during rebound (in the R shear) and post-shearing dilatation (visible in the lower part).

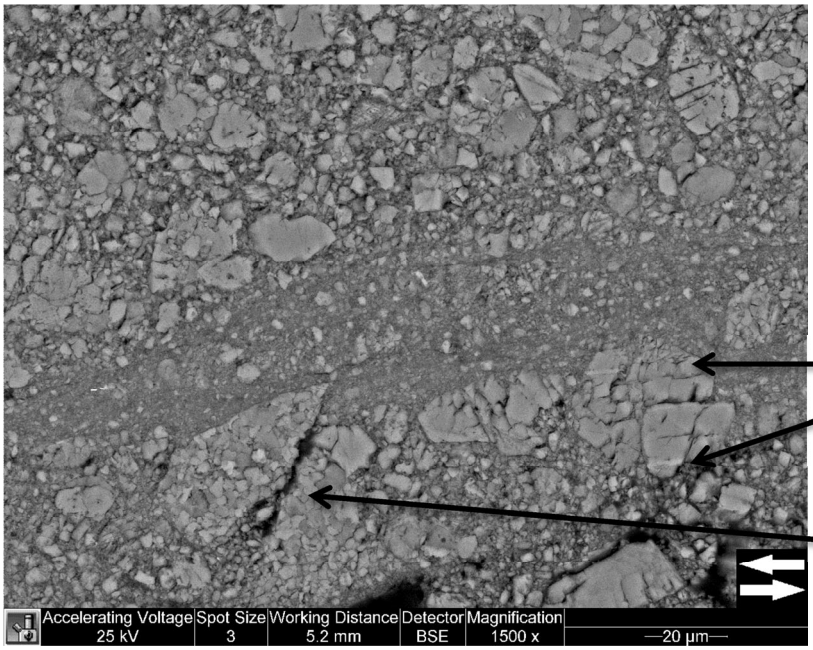

Figure 11: Higher magnification of a R-shear band and intergranular fracturing. The localized shear zone is approximately 20 µm thick, and shows grain size reduction of at least the large grains. Twins are visible and the polycrystalline nature of the "grains" is clearly outlined.

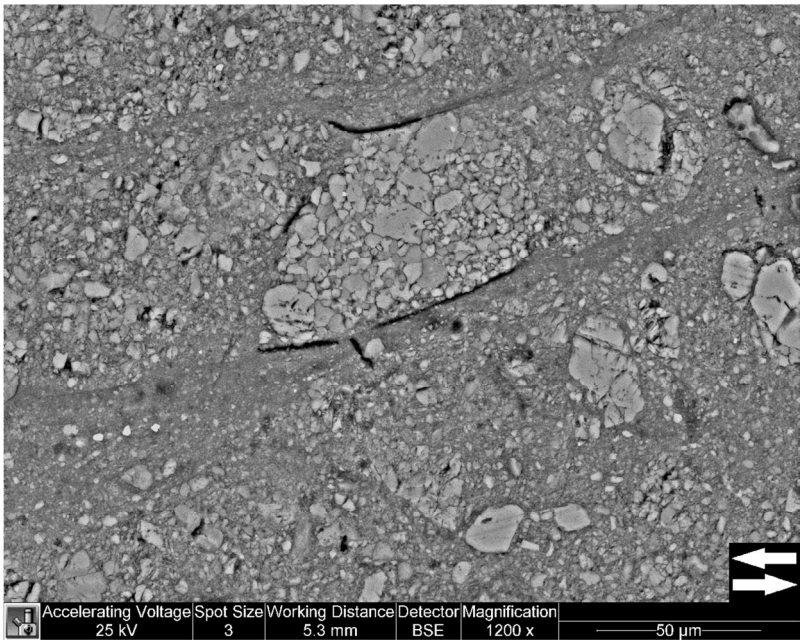

Figure 12: SEM picture of 25°C limestone gouge, showing several R-shears, a clear polycrystalline cluster being affected by the shear band and calcite twins.

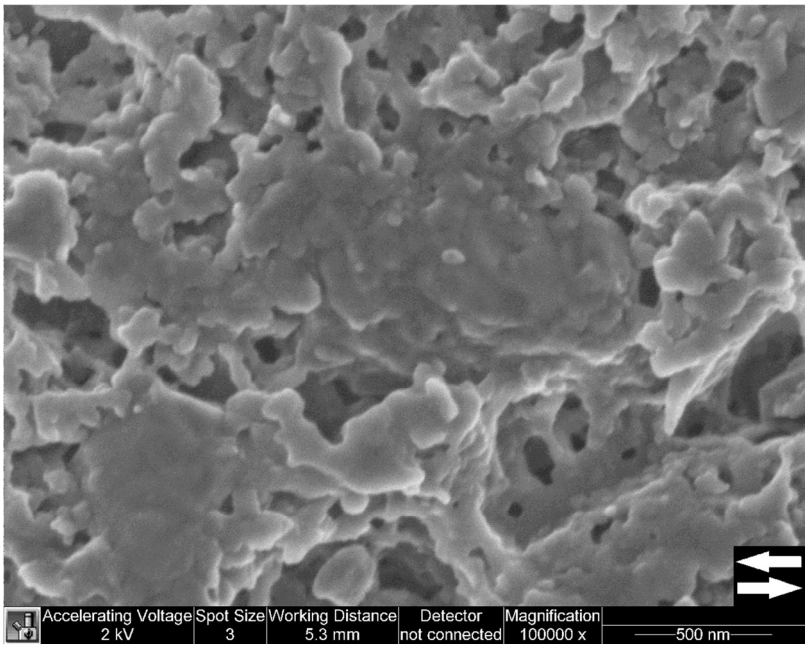

Figure 13: High resolution (high magnification) SEM photograph of the 25°C limestone sample. This photograph is taken in the so-called matrix and it shows the individual grains. These grains are grouped together and individual (loose) grains are rarely seen. Porosity is high and at some locations, the grains appear to be welded (sintered) together.

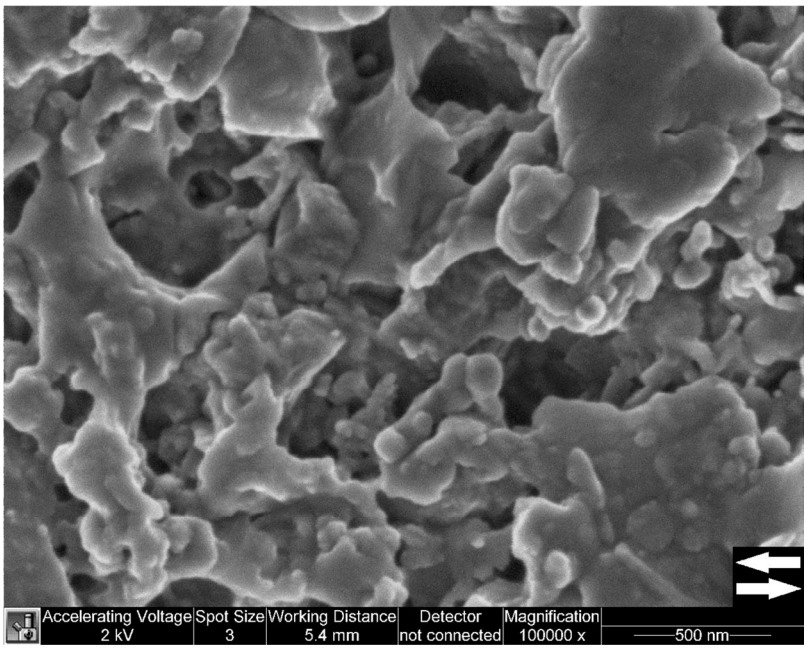

Figure 14: High resolution (high magnification) SEM photograph of the 25°C limestone sample, now more located within a R shear band. Differences to figure 13 are little. Sintering possibly increased, forming elongated shapes. Individual grains mostly still visible and the porosity is high.

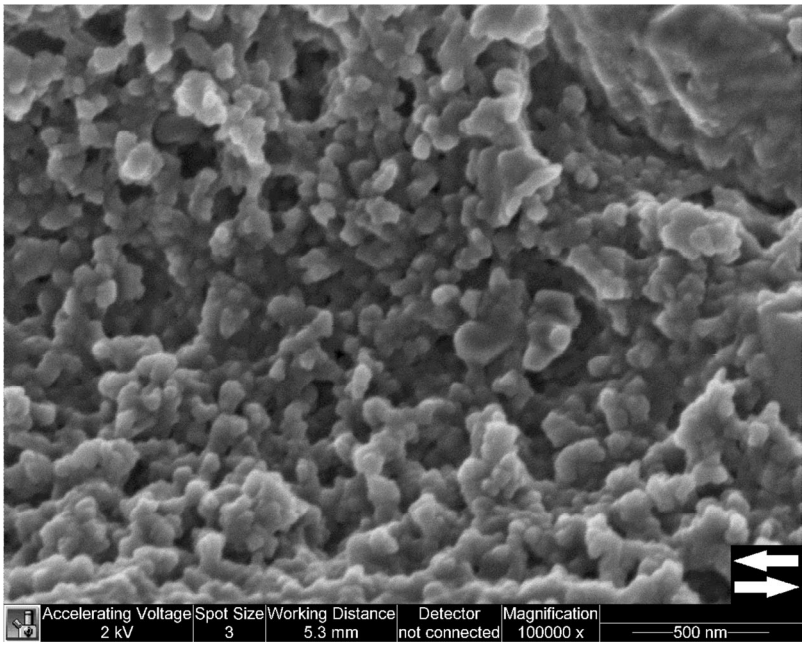

Figure 15: High resolution (high magnification) SEM photograph of the 25°C limestone sample, taken within a Y-shear band at the gabbro boundary. The grains appear to be less clustered. Individual grains very well visible. Grain size does not change significantly from the above figures. Porosity is again high.

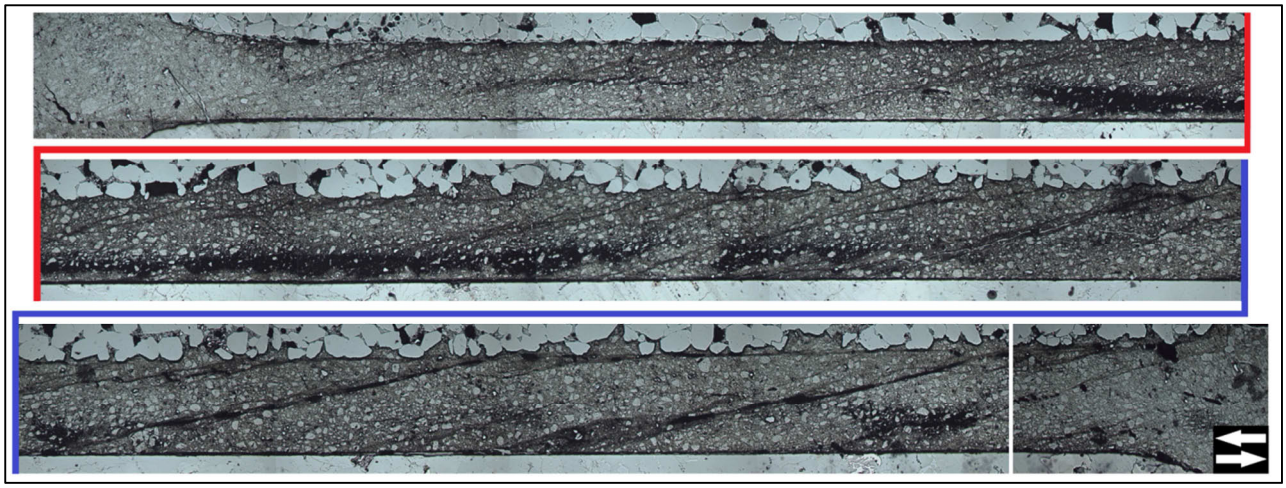

Figure 16: Panoramic photograph made by the optical microscope of the 50°C deformed limestone gouge (sinistral). Set-up is similar to figure 6. Visible is the increase in R-shear bands and again the roughness of the sandstone driver block compared to figure 6.

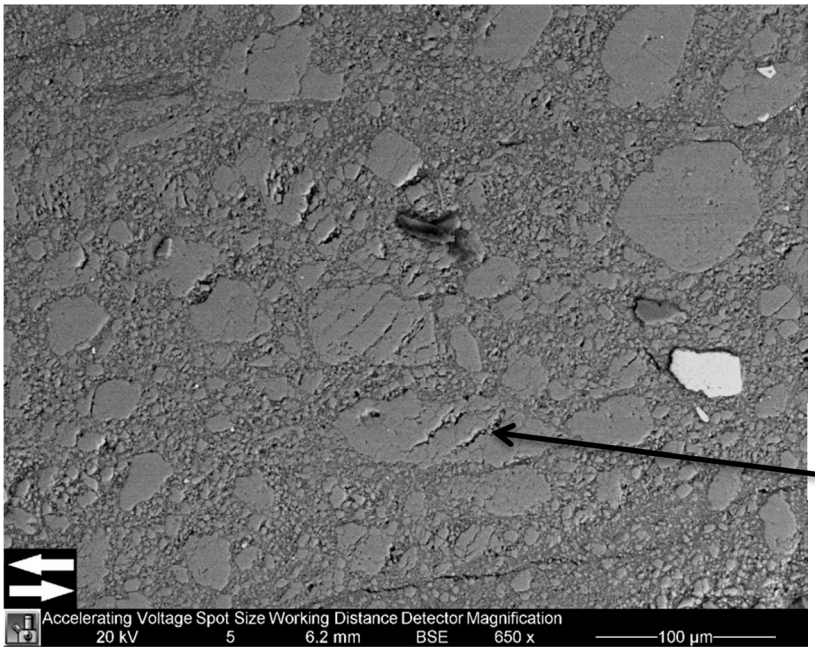

Figure 17: SEM photograph of the 50°C deformed sample, showing intergranular en-echelon fracturing of the large polycrystalline clusters. Photograph is taken at approximately the centre of the sample. Due to probably contrast problems, the polycrystalline nature of the larger grains is less visible compared to the 25°C sample. R shear bands and twinning not visible or not apparent at this location.

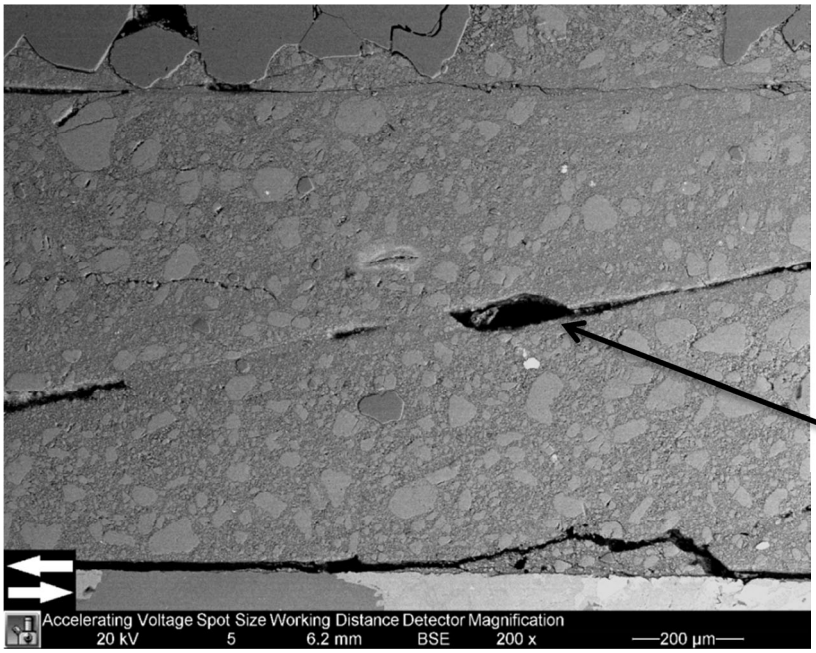

Figure 18: SEM photograph of the 50°C deformed limestone showing a sharp R shear band, with strong evidence for post shearing rebound in the form of a hole due to shear band stepping. Material within the R-shear has probably fallen out during sample preparation, maybe due to the very fine nature of the powder. At the top part, a Y shear is visible, and at the lower part, gaps developed during post shearing dilatation.

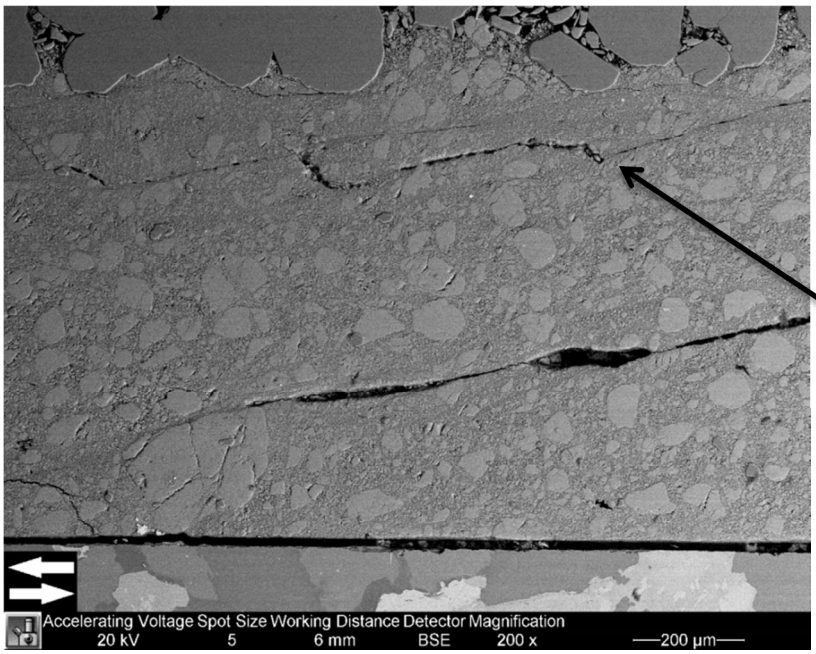

Figure 19: SEM photograph of the 50°C deformed limestone showing again the rebound effect on both small and large scale. Also the Riedel shear density and orientation is well represented in this picture. In the lower left part of the gouge band, a large grain with diameter above 200 µm is located.

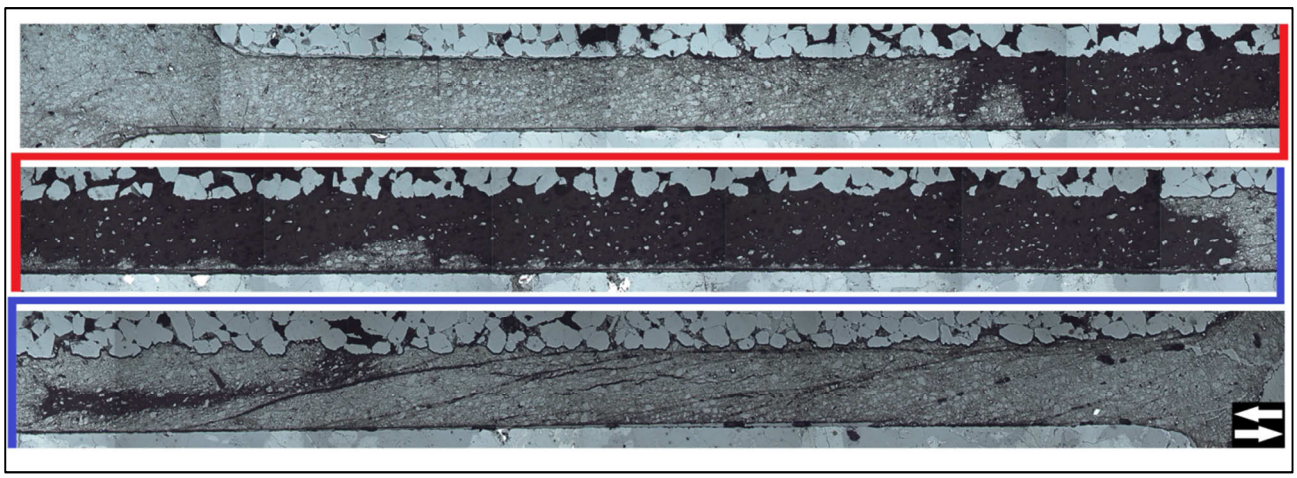

Figure 20: Panoramic photograph made by the optical microscope of the 100°C deformed limestone gouge (sinistral). Transition from rough to sharp sandstone boundary is dark, so microstructural change not well visible. Riedel shear band clearly developed and appears to be deflecting towards the driver block.

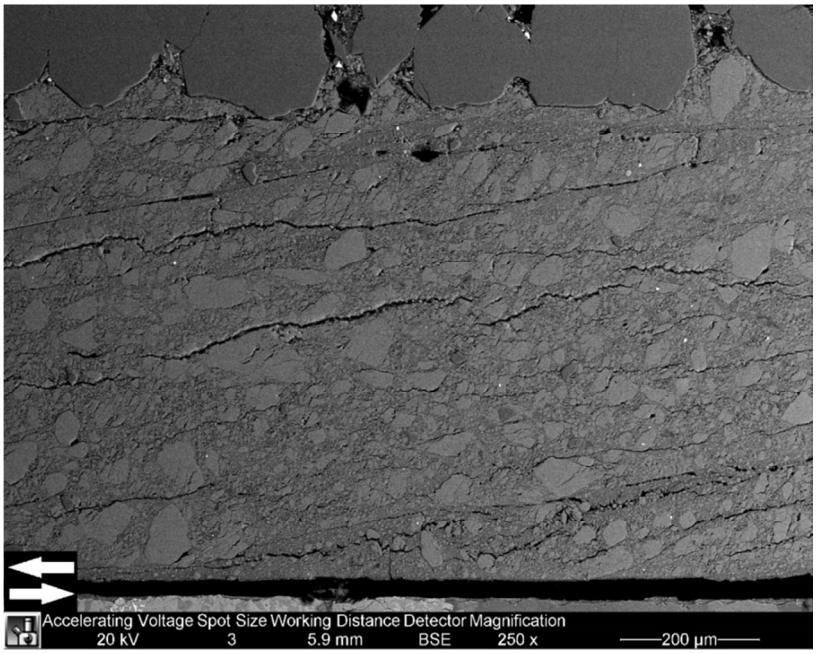

Figure 21: SEM picture at low magnification of the 100°C deformed limestone gouge. Photographs show the large density of fractured grains especially at the upper part of the photograph (near the sandstone driver block). Most of the fractures have the same orientation as the maximum stress direction. Riedel shear bands are clearly visible and dilatation in the form of irregular horizontal cracking is common.

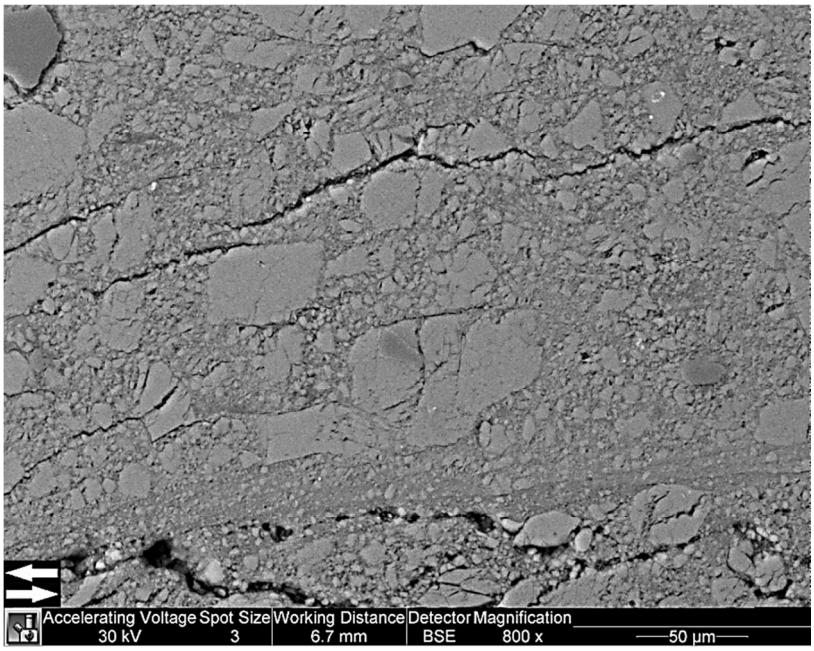

Figure 22: Somewhat higher magnification SEM picture of the 100°C limestone showing parallel R-shear bands forming a wider localized zone (bottom part). The grains are relative angular and appears to be irregularly fractured.

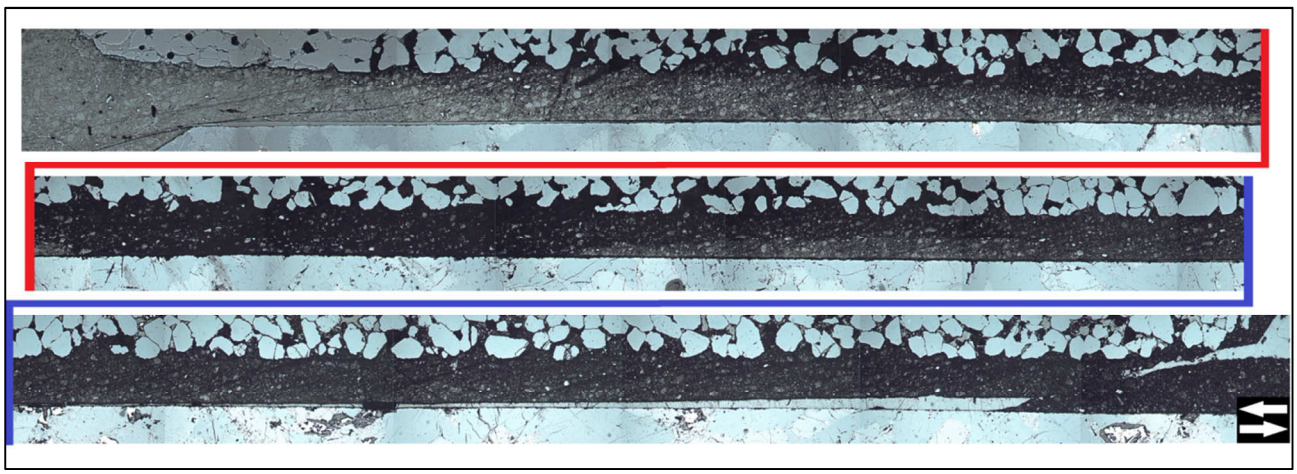

Figure 23: Panoramic photograph made by the optical microscope of the 150°C deformed limestone gouge (sinistral). Whole picture is relative dark. Riedel shear bands visible throughout sample, though they appear to be less developed. Large post-shearing thrust fault (rebound) at the right (lower) part. Twinning is not visible in these panoramas, though they are apparent (see text).

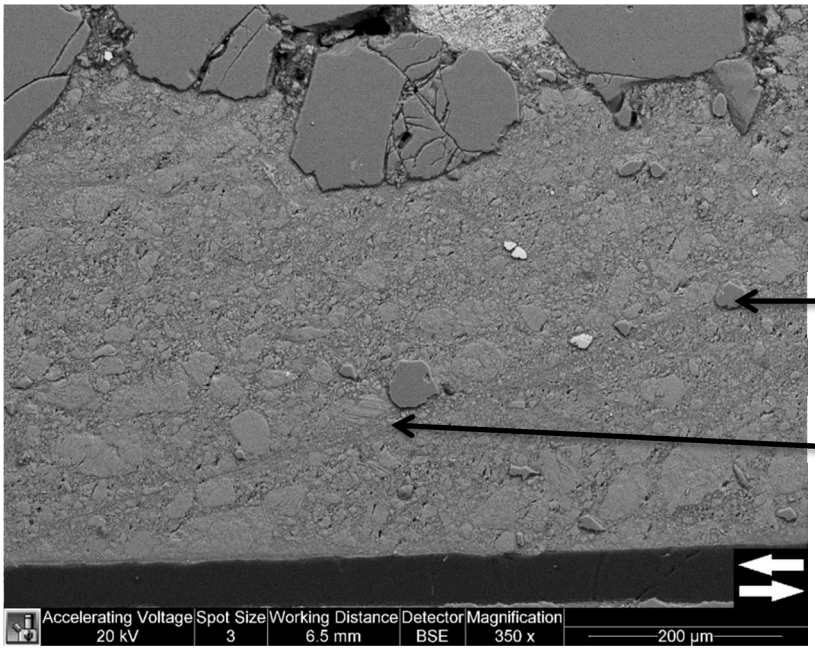

Figure 24: Low magnification SEM picture of the 150°C limestone, showing the chaotic nature of the microstructure. R-shear band is visible but less sharp compared to the lower temperature variants. Twinning is even at this magnification visible.

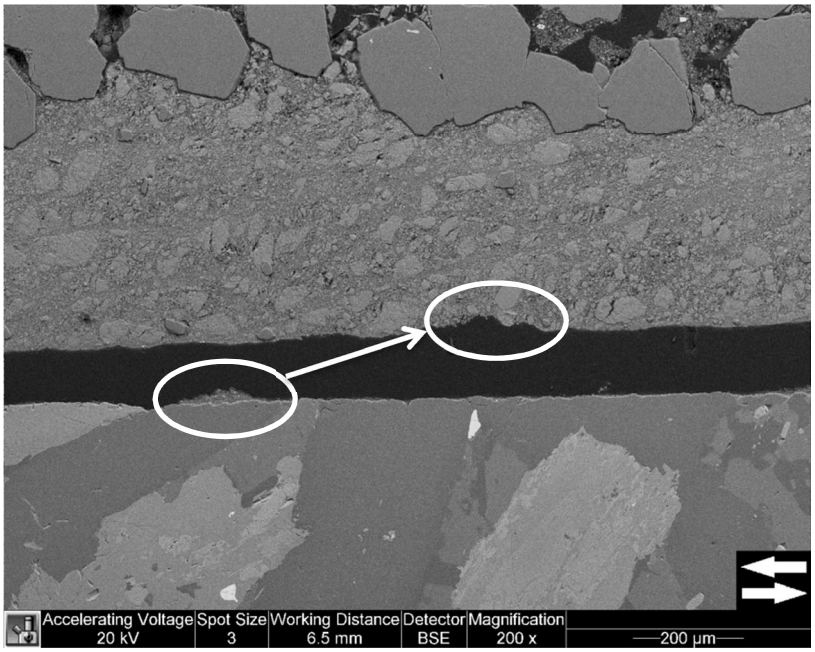

Figure 25: Another SEM picture of the 150°C limestone sample, showing the chaotic nature. Also the significant post shearing vertical extension (~125 µm) and rebound (~500 µm) is clearly visible. The Riedel shear bands are wider and less developed. Intergranular cracking is not as parallel to the maximum stress direction. No Y shearing visible, at least at this magnification.

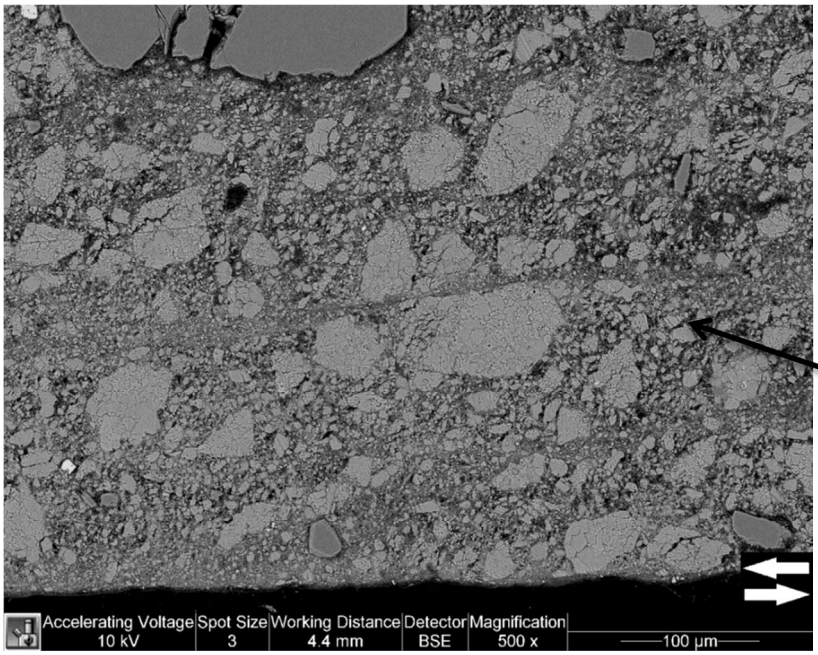

Figure 26: Higher contrast SEM photograph of the 150°C limestone gouge showing the polycrystalline cluster nature and the effect of a R-shear on the cluster. Twins are not common in this photograph, since they are more apparent in the smaller grains (as indicated). The bottom part shows Y-shearing.

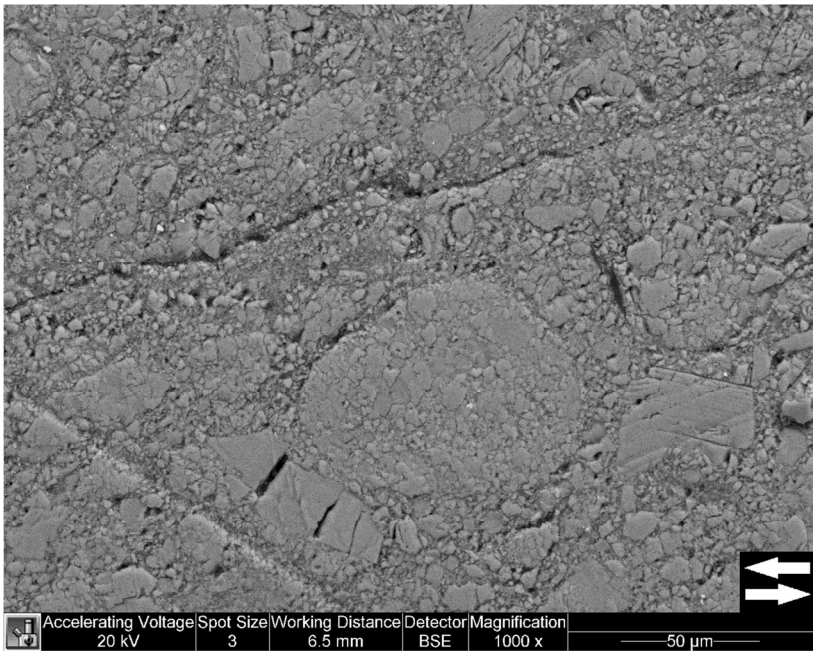

Figure 27: Higher magnification photograph of the 150°C limestone sample, showing the structural differences between the (round) polycrystalline groups and the (angular) twinned grains. These twinned grains are very common and in some cases the twinned grains are fractured along the twins. In general, polycrystalline clusters appear to be more affected by shearing compared to the lower temperature variants.

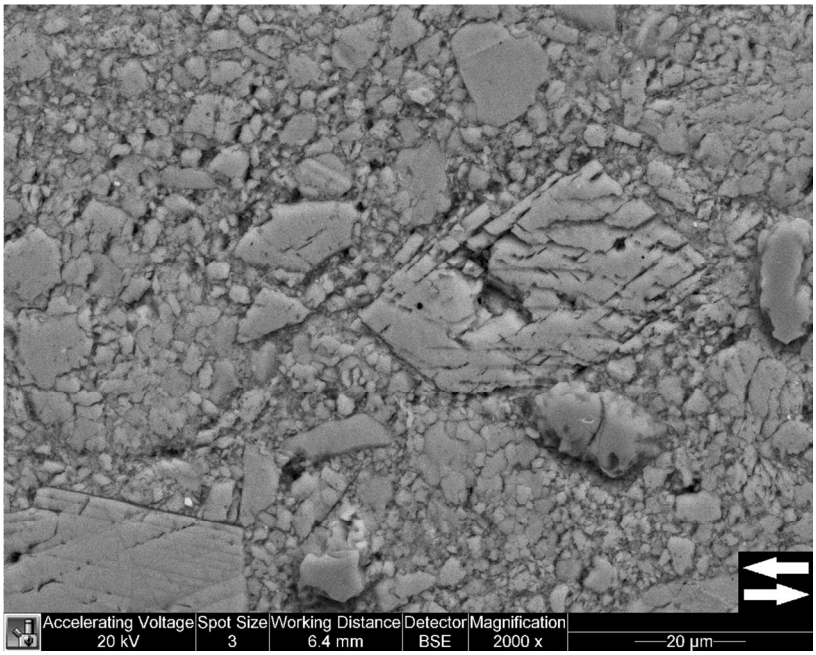

Figure 28: Another SEM picture of the 150°C deformed limestone gouge, showing even better the twinned calcite crystals.

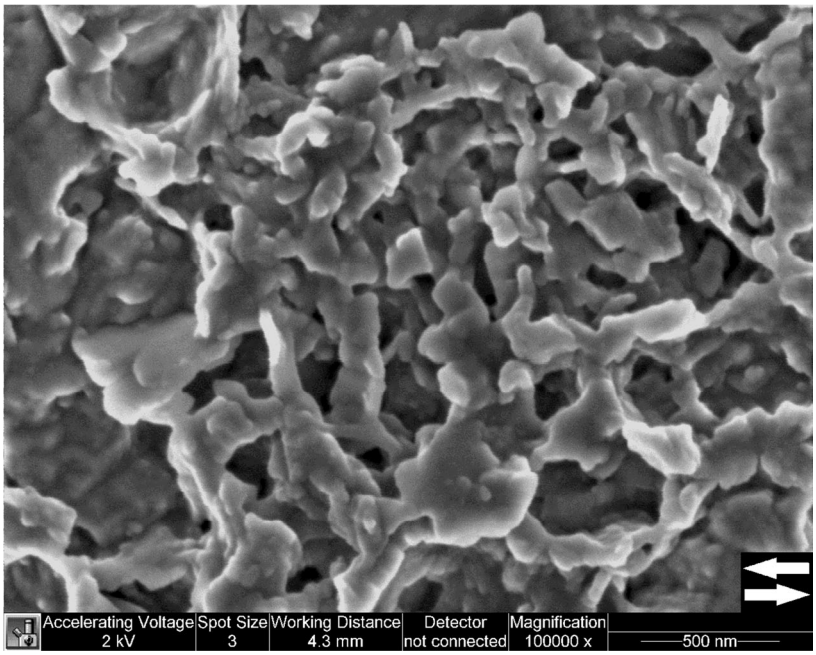

Figure 29: High resolution (high magnification) photograph of the 150°C deformed limestone matrix, showing the elongated shapes the grains produce. The grains are sintered together and the porosity is high. Individual grains are in some cases still recognizable but in other areas only the group shape is visible. Individual grains are relative round and very small (down to 50 nm).

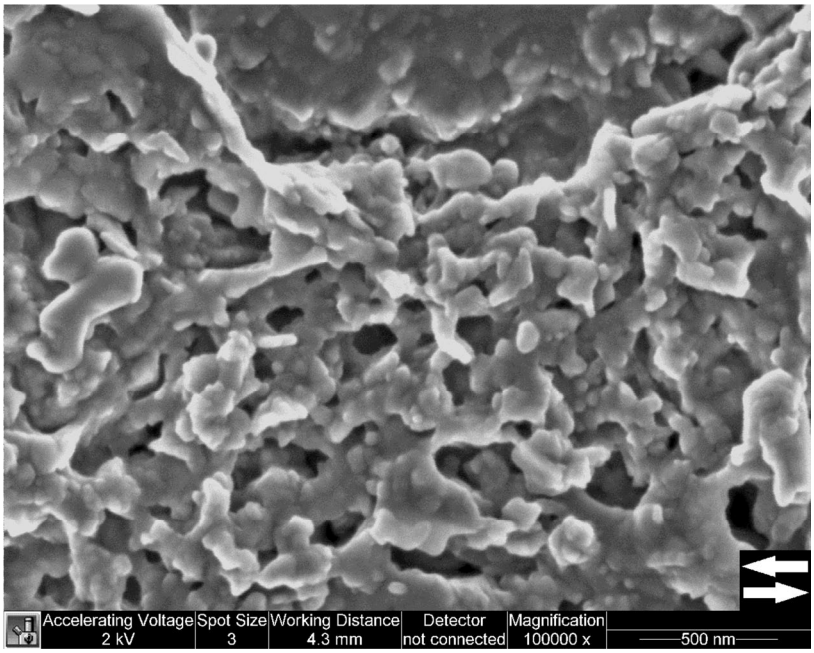

Figure 30: High magnification SEM picture of a 150°C limestone R shear. The microstructure does not vary significantly from figure 29. The sintered character of grains is approximately equal, just as the elongated shape development. Grains are possibly less grouped and porosity might be a little bit lower. At the upper part of the photograph, a part of a larger grain is visible.

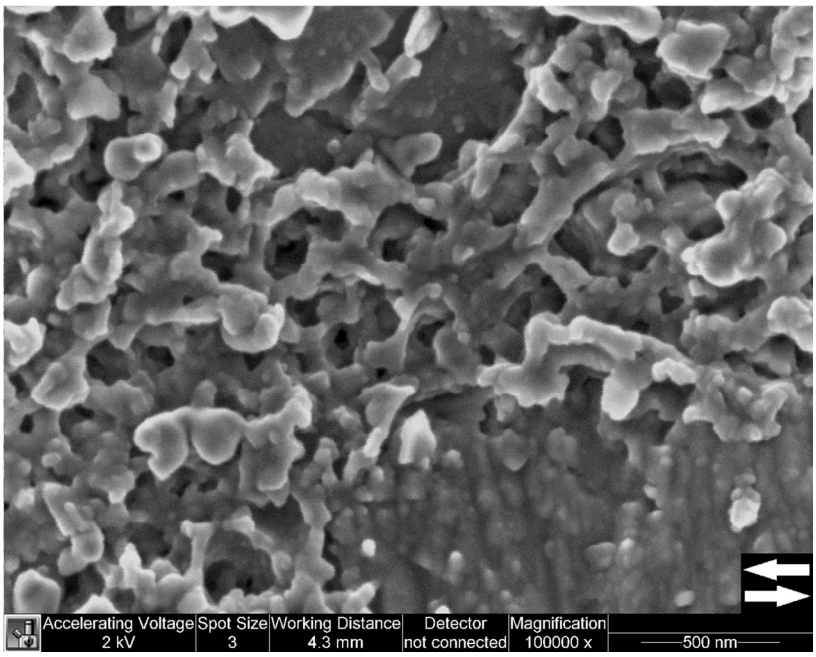

Figure 31: Again a high resolution SEM picture of the 150°C limestone, now taken in a Y shear along the gabbro boundary. Picture shows again the elongated shapes. Individual grains are less visible compared to the low temperature variant. The lower-right part shows (the structure of) a part of a large grain. Please note that the surface of the large grain is not smooth.

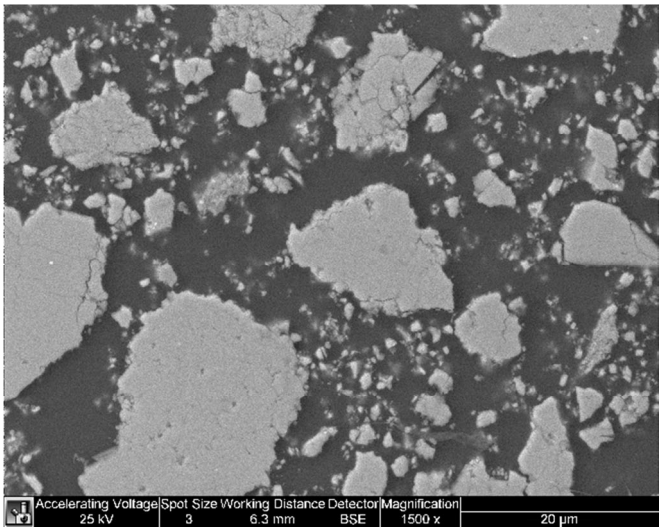

Figure 32

Figure 32 - 34: All three figures show the microstructure of the limestone material (taken by the SEM). The low resolution photograph (left, figure 34) shows the polycrystalline nature of the material and the individual loose material. Twins are not visible. The high magnification pictures (figure 33 and 34 below) show the microstructure of a polycrystalline cluster and the possible individual grains which make up the matrix in the sheared variants. The bridging character is not found, but the grains are forming elongated bacteria-like shapes (figure 34). Comparing it with the sheared samples is difficult.

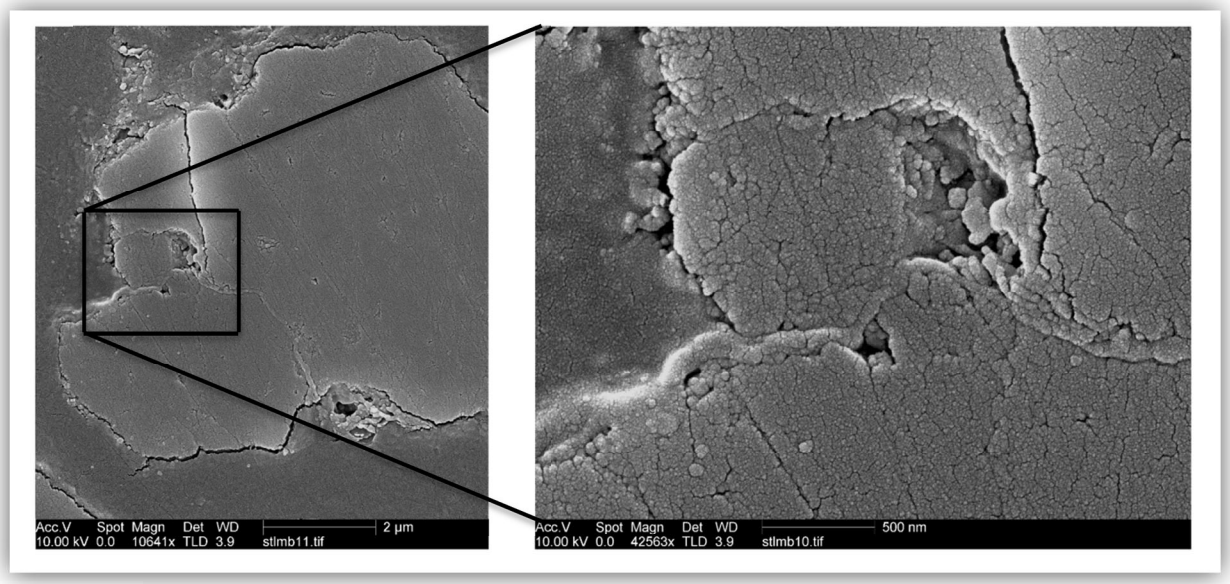

Figure 33

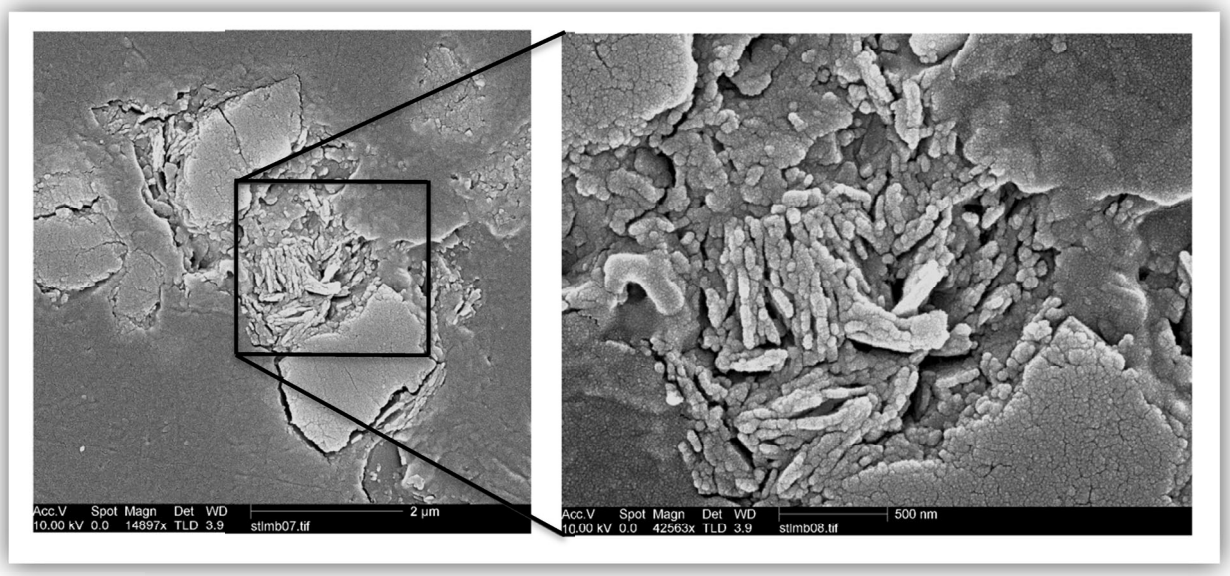

Figure 34

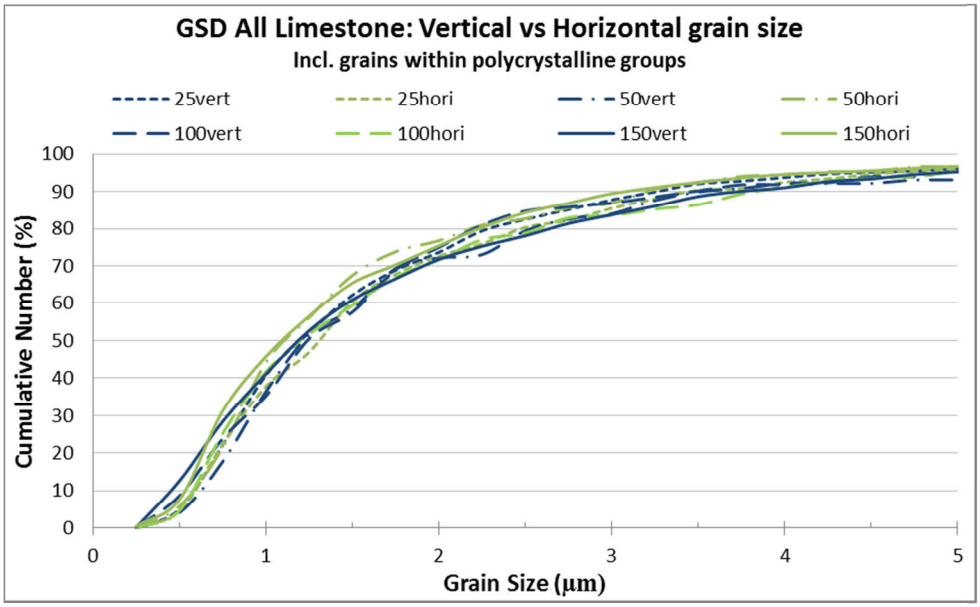

Figure 35: Graph showing the grain size distribution of all the limestone grains, including the grains within polycrystalline groups. The grain size is normalized to 100%. The green (dotted) lines are the horizontal grain sizes and the blue data represent the vertical grain sizes. The graph might show a slight trend of the horizontally measured grains being smaller than the vertical measured grains. This trend is likely to be insignificant. Please note the small grain sizes. Number of grains measured: 2547

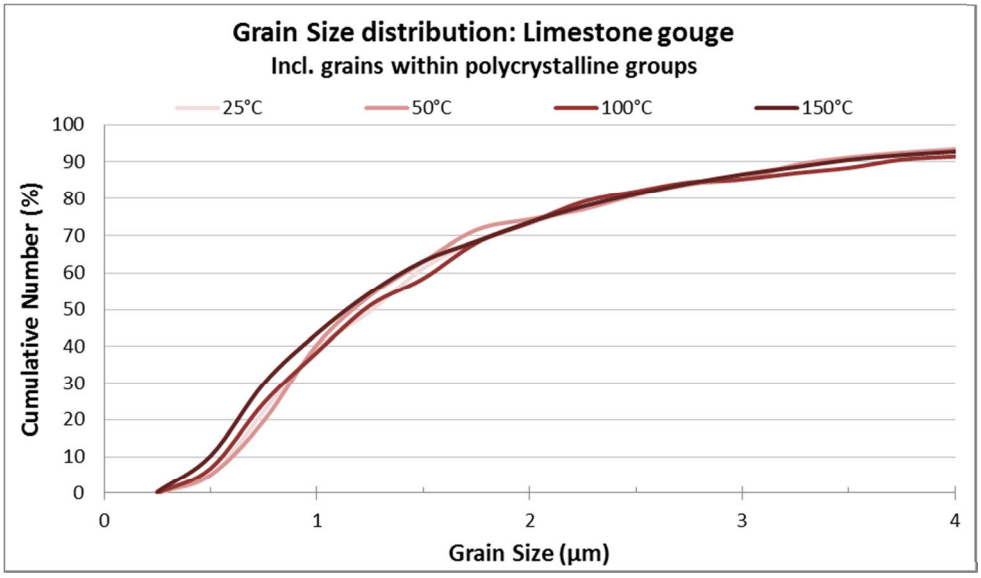

Figure 36: Graph is approximately similar to figure 35, with the difference that the horizontal data and vertical data are taken as one group, so that this graph shows the temperature variations better. As visible, these variations are only little. The highest temperature limestone sample appears to have the smallest grain sizes, but grain size reduction, including all the grains is possibly only small. Number of grains measured: 2547

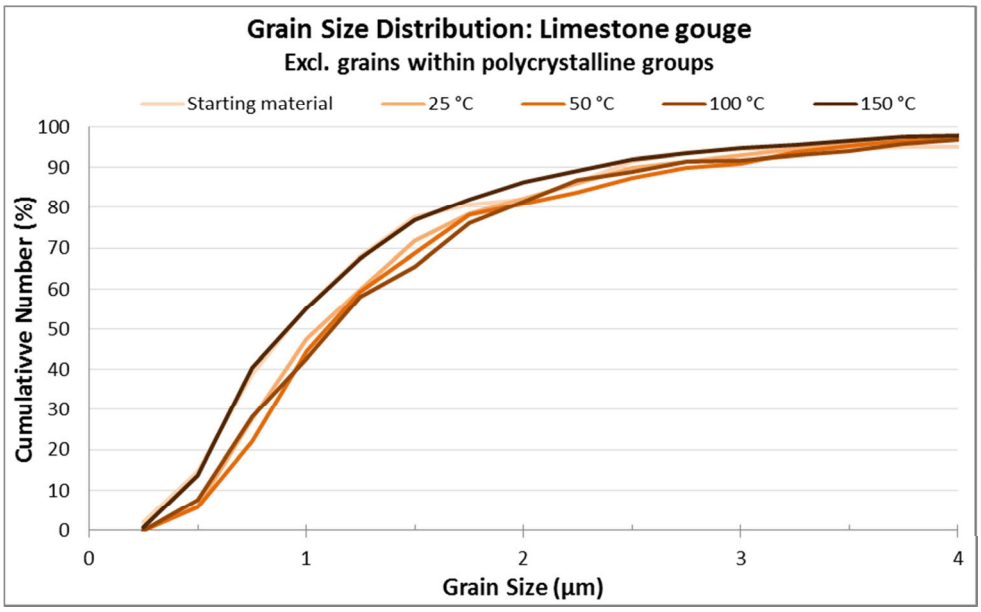

Figure 37: Graph approximately similar to figure 35, with the exception that the grains within the polycrystalline groups are now excluded, whereas the starting material grain size is included. The figure does not show any grain size trend, except that the 150°C sample has finer grain size compared to the other variants. So grain size reduction does either not took place or only little (beyond observable limits). Number of grains measured: 1796

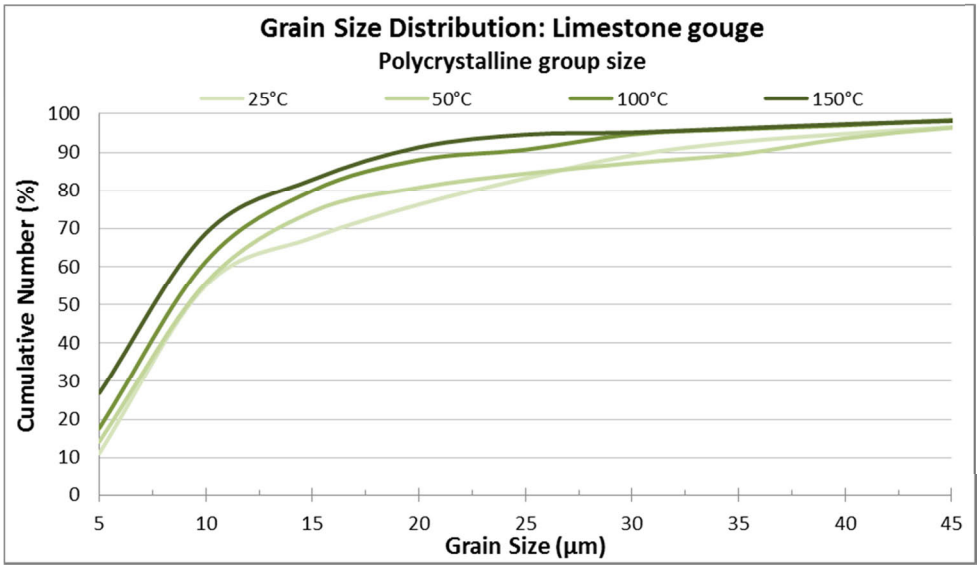

Figure 38: Graph showing the size change of the polycrystalline groups. During shearing, these groups act as individual grains. The "grain-size" decreases significantly with higher temperature. Please note the starting material is not inserted in this plot and that the grain size is a factor higher compared to the individual grains. Number of "grains" measured: 1177

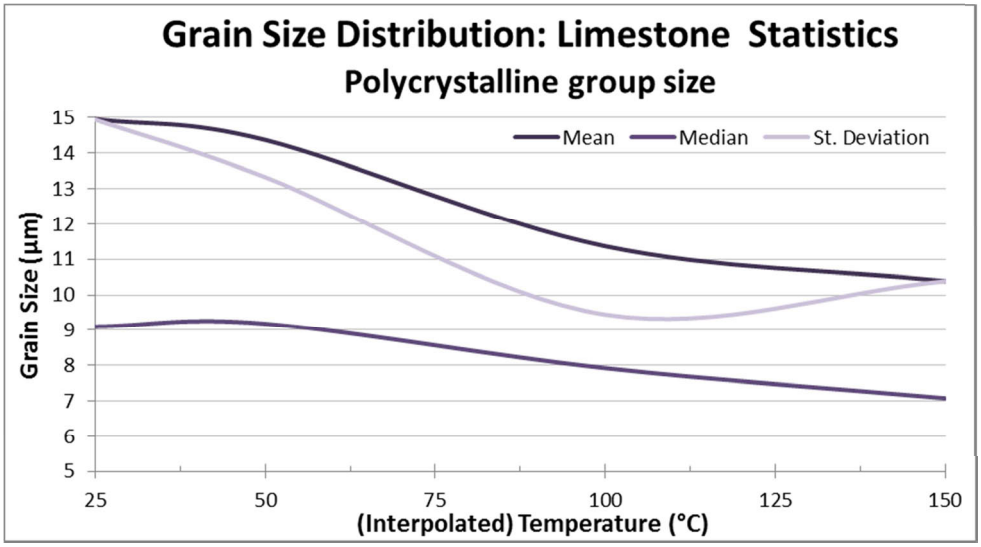

Figure 39: This graph is based on the data equal to figure 38. The mean, median and standard deviation are plotted in a grain size versus temperature diagram to show the grain size development with temperature. Both the mean grain size and the median size decrease with increasing temperature. Number of "grains" measured: 1177

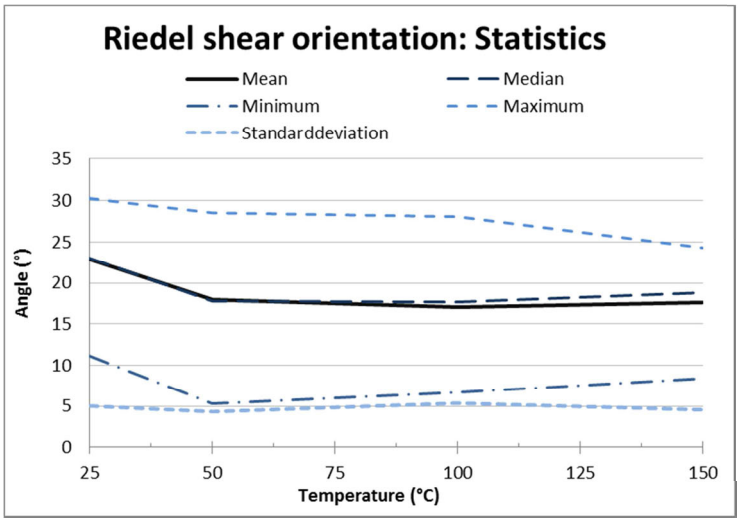

Figure 40: R-shear band orientation analysis. Both the mean R-shear orientation and the maximum angle decreased with higher temperature. On the other hand, the minimum angle increases. For discussion and further comments on the results, I refer to the text. Number of R-shear bands measured: 137

4. Discussion and comparison to previous literature

The aim of this report is to investigate the microphysical mechanisms and microstructures acting and developing in a simulated limestone gouge, in order to determine the process or a combination of processes causing the observed velocity weakening at elevated temperatures. In this discussion session, I will go further into detail on the obtained results. This includes additional information from past studies. This comparison is needed to obtain insights in the microstructural processes that might have played a role in the development of the microstructures observed and mentioned in the results section, and finally, both the results and background information are used to develop more insights in the microphysical process causing the velocity weakening in the high temperature limestone gouge. I will look at the effect of twinning, R-shear development, pressure solution, compaction/dilatation and the grain size distribution variations within the different limestone gouges.

4.1. Previous studies: Velocity weakening

Rock friction studies have been executed in many ways. Verberne et al. (in press) performed a low velocity experiment, with a maximum shear displacement rate of 1.22 µm/s. This study is based on the velocity weakening found in the limestone gouges deformed at these low shear displacement rates. The frictional properties of rocks at low slip rates (<0.01 m/s), as done for this study, has long been studied in detail in laboratory experiments as reviewed in Marone (1998). Strong velocity weakening has also been found in several cases by fulfilling high-velocity friction tests (either by a friction welding machine or a high-velocity rotary-shear friction testing machine (e.g. Mizoguchi et al, 2009; Han et al., 2010 and references therein) on for example simulated carbonate gouges. The slip rates reach up to a maximum of 1.60 m/s (Han et al., 2007a; 2010). They propose that thermal decomposition of carbonate fault gouge might be an essential process for the fault weakening. Calcite decomposition is the (endothermic) breakdown of calcite into aggregates of CaO nano-grains and CO_2 (Han et al., 2007a; 2007b and Sulem and Famin, 2009). The weakening is then likely to be occurring due to powder lubrication by the developed nano-grains instead of pressurization of CO_2 due to the high porosities in the gouges, which might be even possible for low velocity shearing experiments. However, this calcite decomposition cannot be occurring during the experiments conducted by Verberne et al. (in press). The temperatures reached in the high velocity experiments are a factor of 10 times higher than the maximum temperature of 150°C, with a resulting frictional strength of the material significantly lower than in this research. Dieterich (1979a) mentioned the effect of healing of the material at lower velocities, causing the significant strength drop at high sliding velocities. On the other hand, nano-grains are present in a significant amount in the limestone samples and sliding over them is also without calcite decomposition possible.

4.2. Riedel Shear bands

One feature which differs significantly within the limestone gouge compared to the other gouges is the appearance of en-echelon arrays of Riedel shear bands (see results section 3.2. and 3.3.). Riedel shear structures are first studied and reported by Riedel (1929), by the use of clay-cake experiments. Riedel shear bands are recognized as thin zones of localized deformation that takes place as simple shear (Kolymbas, 2009). These structures are found at any scale (from micro-scale, as developed here, to plate contact scale), and are associated with general strike-slip displacement (e.g. Katz et al., 2002). Riedel shear bands are fracture networks with different orientations. The (often) most developed shear band is the R shear (also known as the R_1 shear). These shear bands are synthetic to the shear sense. The antithetic R' (also known as R_2) shear bands dip more strongly in the same direction whereas P-shears are opposite (mirrored) to the R shear bands. Parallel to the shearing direction, Y shear bands might develop. In this study only R

and Y shear bands are recognized. The angle of the R shear band with respect to the shearing direction is related to the angle of internal friction (φ) in the form of φ/2 (Katz et al., 2002). In the present study φ = 35° - 45°, dependent on the sample. Despite the intense study on Riedel shear bands, the mechanical nature of Riedel shears is not completely known. In this study, only R and Y shear bands are found (see figures mentioned in results section 3.2.). If the R bands are purely shear bands with no structural accommodation at the ends, geometrical problems will be significant. Gaps are expected to develop at dilatational spots and squeezed material is expected where material is pushed towards. Reorganization of individual grains is needed to account for this. Another way to partially account for this accommodation problem might be to flatten the already developed Riedel shear bands. It is expected that the amount of sliding over these bands increase during the shearing process, and to compensate for this, the shear bands rotate to avoid large gaps at the ends. This rotation is also slightly observed during the R-shear orientation calculations.

Since the other gouges do not show significant Riedel shear bands whereas the limestone gouges are filled with them, it is likely that these Riedel bands are related to the velocity weakening. They act as localized zones over which sliding might become easier. Due to the lack of large grains, the mean grain size within the shear bands (both the Y and the R) is decreased. This makes rolling or sliding over the resulting (nano) grains easier, decreasing the strength of the material. How much the shear displacement over an individual shear band is, is not examined (yet) making it impossible to say whether the Y and R shear bands accommodate the whole shearing motion, causing the so-called matrix to be static, or whether the displacement on the localised shear bands is only little so that the influence of these shear bands is small too. The widening of the shear bands of the 150°C limestone sample makes rolling over each other easier. Why the velocity weakening process does not occur for the low temperature variants cannot be solved on the basis of this information.

4.3. Calcite twinning

Temperature dependent crystal plastic deformation was indicated by Verberne et al. (in press) to be a possible mechanism causing the velocity weakening. In (coarse grained) limestone and marble, mechanical (e-)twinning of calcite is the dominant mechanism of crystal plastic deformation and searching for twin development in the simulated limestone gouge is therefore necessary to examine plasticity. The most important twinning systems in calcite are slip on the e, r and f plane (Bresser and Spiers, 1990; 1996). At low temperatures (as is in this paper), it is easiest to glide on the e-plane (Bresser and Spiers, 1990). From light and electron microscope observation, I noticed an increase in twinned grain density within the limestone gouge. However, several problems arise when interpreting this. First of all, the visibility of the twins is difficult in both reflecting light optical microscopy and BSE electron microscopy. The samples are too thick for transmitted light and too smooth for the SE detector at low magnifications. The starting material also shows calcite twins thus at least a part of the sheared gouge twins must be inherited. Despite this, the micrographs show an increase in e-twinning with higher temperature thus the process of twinning must be at least slightly temperature dependent. Ferril et al. (2004) used the calcite twin morphology to determine the temperature dependency. Twins in calcite develop at temperatures below 400°C and initiate at low shear stresses (Fredrich et al., 1989). Above this temperature, recrystallization takes place and twins will be erased. At temperatures below 170°C, only thin twins are expected to develop, with twin-thicknesses of less than 1 µm thick. Most of the twins apparent in the 150°C limestone (figures 26-28) gouges are twins of this size, thus they might be developed during shearing. Thick twins are apparent in all the sheared gouges and are likely to be inherited. Despite this, the temperature dependency of twins to develop is very small and twin intensity and thickness is more related to the differential stress the material underwent, which was equal for all the sheared material in this study (Rowe and Rutter, 1990). Based on the above, it is

possible that the development of twins as a mechanism of crystal plastic deformation might trigger velocity weakening. When knowing the twin density due to this specific experiment, strain rate due to calcite twinning only can be (roughly) determined or estimated. If this is known, it can be determined what the effect of twinning is on these limestone gouges. The other gouges do not have (as much) calcite, thus calcite e-twinning is not or less possible. (E.g.) the mudstone does not show any twins and it neither showed velocity weakening.

4.4. Grain Size Distribution (GSD)

From the results section (3.4.) and figures 35-39, you can see that the grain size for the smaller grains does not decrease with increasing temperature/strain. This could have multiple reasons: first of all, the size of the grains did not decrease, but also the effect of magnification could have played a major role. From high magnification photographs it is visible that the grain size decreases down to 50 nm for the limestone gouge samples. These grains are not visible in the 1500 times magnification photographs at which the grain size distribution is determined. The nano-grains are probably taken in groups or appear as the darker so-called "matrix". The smallest groups visible are most likely measured instead of the individual grains. However, when looking at the pictures at high magnification, the grain size does not seem to decrease significantly. The polycrystalline groups on the other hand do decrease in size with higher temperature. These larger "grains" are more easily affected during shearing and are thus easier to fragmentize. One major consequence of cluster-size decrease is the volume increase of the very fine (nano) matrix. The polycrystalline groups are less obstructing the R-shear bands compared to the low temperature variant, with the result that these localization bands might become wider, as visible in the photographs. Fault gouges evolved in low temperature and low pressure zones often developed due to cataclasis, which is the process of continuous fragmentation (fracturing, crushing, chipping, sliding, rotation and grinding) of particles and according to Storti et al. (2003) the remnants controls the frictional fault properties as well. These authors also mention the tendency for cataclastic rocks to develop a self-similar grain size distribution having a fractal dimension D of 2.58. As mentioned, the fractal dimensions are not calculated here. Cataclasis has the consequence that relative large grains tend to become rounder compared to small grains (Storti et al., 2007). Very small grains as encountered in this study are less affected. The relative strength for smaller grains is high and grain size reduction is less likely. Due to this small grain strength, the grain size does not continuously reduce during faulting and shearing, which could be the case in this research for the small (individual) grains. Therefore it is expected that grain size reduction or increase in general does not play a major role in the shear zone evolution and consequently, it probably does not have a major effect on the velocity weakening. On the other hand, it is more likely that the fine grained nature itself plays a bigger role, as will be more outlined later in this discussion section.

4.5. Compaction or dilatation?

The compaction/dilatation results show a clear contradiction: the high resolution SEM photographs (figures 13-15 and figures 29-31) do not show complete compaction, independent on the location within the sample, whereas the calculated compaction analysis (table 2) provides the result of compaction of the 150°C with respect to the 25°C limestone gouge. The principle deformation mechanisms controlling compaction are intergranular sliding, grain fracturing, grain plasticity (dislocation glide, twinning) and intergranular pressure solution (IPS) where IPS is the dominant compaction mechanism at low (room) temperature and low stresses (Zhang and Spiers, 2005 and Passchier and Trouw, 2005). However, it is very difficult to correlate the contradictory results, thus the process controlling compaction or dilation cannot be determined directly. The difference could be due to incorrect compaction calculations. The error of this calculation is relative high due to uncertainties. The gouge porosity at the gouge bands ends and

the squeezed material is unknown. This gives difficulties in determining the volume of the material, since homogeneous porosity/density is assumed for the calculations. It is also unknown how the material has acted during shearing in depth. The thin section is just a slice of a 3D sample and the gouge material was most likely also squeezed into the third dimension. There are no calculations or corrections made, based on 3D effect. Due to the uncertainties, it is possible that the material has not been significantly compacted at all, and from observations, (local) dilatation probably took place during shearing. Therefore, the post-shearing dilatation due to the FEP tubing is also relevant. The lack of (significant) compaction should not give problems with interpreting this together with the process of velocity weakening. Niemeijer and Spiers (2006) investigated the velocity dependence of strength of phyllosilicate-bearing fault gouge instead of limestone gouge. They argued that in the velocity weakening regime, the gouge has to dilate to accommodate slip whereas in the velocity strengthening regime is marked by pressure solution, healing, and foliation development (due to phyllosilicate wrapping). This relation between dilatation and velocity weakening is combined with the development of a "chaotic" cataclastic fabric. The dilatation is thought to be caused by granular flow instead of intergranular sliding.

4.6. Pressure solution

Pore fluid assisted dissolution-precipitation processes might play a major role in the microstructural development of the limestone. As discussed before, it has been recognized as an important mechanism causing compaction in the upper and mid crust (Zhang et al., in press and references therein). Many studies have been executed on the dissolution and precipitation properties in general and on calcite more specifically (e.g. Rutter, 1983; Zhang and Spiers, 2005 and Zhang et al., in press). Pressure solution is controlled by three kinetic processes: dissolution, mass transfer (diffusion) and precipitation. Zhang and Spiers (2005) showed the dependency of, for example, grain size on the strain rate caused by pressure solution. The slowest of these three steps is the rate controlling step. An increase in particle size decreases the strain rate (e.g. Zhang et al., in press). This is because the relative grain surface decreases with the result that the rate of dissolution and precipitation is lower so that the reaction rate might become more limited. Evidence for precipitation and/or dissolution in the limestone gouge might be found as sintered grains. If true, this could be either related to the dissolution at the grain contacts, causing a sort of "fusion" between grains, or it might be related to the precipitation of calcite at free grain contacts. This latter explanation can also develop the sintered character. Remarkable is that this sintering is found predominantly in the 150°C sample and less in the low temperature variant, since it has been proposed by Niemeijer and Spiers (2006), that the relative effect of pressure solution decreases with higher temperature whereas the possibility of an increase in "sintering" observed in the samples should imply a relative increase with higher temperature. Please note that according to Zhang et al. (in press), the effect of the decrease of IPS with temperature is only small and that a decrease in grain size (as observed) increases diffusion. On the other hand, the chaotic structure developing in the velocity weakening regime and the better developed microstructure (e.g. the sharp R shear bands and the mode I cracking) in the velocity strengthening/steady state regime corresponds with the Niemeijer and Spiers (2006) study. This chaotic structure includes the lack of sharp R shear bands, no grain preferred orientation and no preferred shape. Please note that the layered like structure found in the high resolution photographs might be due to sample preparation. Due to continuous polishing of the sample, the surface might be affected forming the structures as visible.

4.7. General model

Bearing all the microstructural observations in mind, it is very difficult to fit the data with a general model explaining velocity weakening in the limestone gouge at 150°C. However, Niemeijer (2006) produced a model which predicts friction

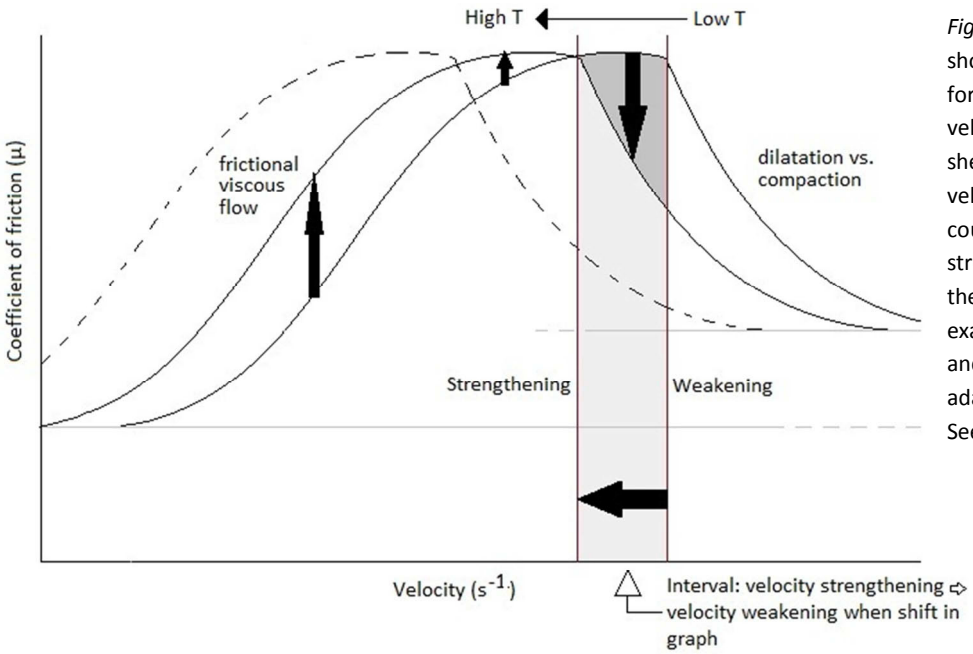

Figure 41: Schematic model showing the three regime model for velocity strengthening and velocity weakening against shearing velocity. At constant velocity, the nature of the material could change (from e.g. strengthening to weakening) when the graph is shifted due to for example temperature variations and pressure solution. Figure adapted from Niemeijer (2006). See text for discussion.

coefficients (versus strain rate) for a quartz-phyllosilicate gouge at constant stress. This model consists of three parts: (1) the low velocity model showing velocity strengthening due to frictional (sliding)-viscous flow. (2) The high velocity model, showing velocity weakening due to a dilatation (rolling) versus compaction (pressure solution) struggle. The third (3) part is the intermediate part, being a balance between the two parts.

Niemeijer (2006) showed that at higher temperatures, the friction coefficient plot will shift to higher strain rates, thus at constant strain rate the higher temperature gouge is stronger in the velocity weakening regime and weaker in the velocity strengthening regime. At the strain rate zone where the high temperature variant is still in the velocity strengthening regime and the low temperature already in the velocity weakening regime, a transition from velocity strengthening to velocity weakening is expected when elevating the temperatures. Assuming the model shape is approximately equal for the limestone gouge, this kind of transition might explain the velocity weakening observed for this study. A decrease in pressure solution (with higher temperature) weakens limestone, shifting the curve towards the velocity weakening regime at the intermediate part (2). The strength curve shifts to the right with temperature, but depending on the effect of the pressure solution, this will counteract (at least partially) the temperature dependency of the material, so that net the curve might become shifted to the left (figure 41), where the material becomes velocity weakened in the centre part of the curve when the temperature increases.

On the other hand, crystal plastic flow in general is also a mechanism for compaction. A similar plot as figure 41 might be expected if crystal plastic flow is the most important compaction process. Plastic flow generally hardens the material at low velocities. With higher velocities, strain cannot be accommodated by plastic flow only and compaction should then be counteracted by dilatation, similar to the Niemeijer (2006) model. However, there is no evidence that significant amounts of crystal plastic flow took place since there are no elongated (plastically deformed) grains present. The 100°C-150°C limestone gouges could then just be the transition from staying strong to becoming weakened, with the microstructural consequences observed under the microscopes. Also the nano-gouges, present in the limestone gouge, could easily cause powder lubrication, which accelerates diffusion enormously by providing a fast diffusion path.

How the model looks like in detail is unknown, but it is likely that the model shown in figure 41 shows the model outline belonging to the limestone gouge, where the 100°C-150°C limestone gouges could then just be in the

transition from staying strong to becoming weakened, with the microstructural consequences observed under the microscopes.

5. Conclusions and further recommendations

5.1. Summary and conclusions

The goal of this study was to examine the microstructure of four types of fault gouges: a simulated natural gouge, and three simulated sedimentary gouges including sandstone, a mudstone and a limestone gouge. Since velocity weakening was discovered for the limestone gouge at 150°C, the focus lay mainly on finding microstructural evidence on the processes causing the velocity weakening. The main observations and the microphysical processes are shortly summed below:

i. Both the starting material and the sheared variants of the limestone gouge show the polycrystalline nature of the material. These polycrystalline groups probably act as individual grains, showing a slight grain size reduction with increasing temperature.
ii. By looking under both low and high magnification and by GSD calculations, no (significant) grain size reduction (or increase) of the individual grains have been found.
iii. Riedel shear bands have developed in significant amounts (within the limestone gouges), becoming increasingly common with higher temperature up to 100°C. R-shear bands in the 150°C sample are harder to distinguish, less sharp, less ordered and thicker compared to the lower temperature variants. The amount of displacement along a Riedel shear band could not be determined
iv. At higher temperatures, R-shear bands appear to deflect towards the gabbro driver block.
v. The 150°C deformed limestone gouge appears to be more chaotic, having no (visible) type of grain preferred orientation or fracture pattern. The grains are more angular in shape and the layer is significantly thinner than the lower temperature variants.
vi. Despite the difficulties in recognizing calcite twinning and having them in the starting material, it appears to be that twinned grain density increases with temperature.
vii. Based on photographs, pressure solution appears to be more significant with higher temperatures. Earlier research showed that this should be the other way around.
viii. The other gouges show little differences between the low and high temperature variants but major differences compared to the limestone gouge. R-shears do not develop (in significant amounts), twins are not apparent and there is no (clear) evidence for pressure solution (due to the low magnification).
ix. Pressure solution (and crystal plastic deformation) causes compaction whereas grain-rolling causes intergranular dilatation. Both slight dilatation (by looking at the pictures) and compaction (by calculations) could be the case in the high temperature sample. The struggle between (intergranular) dilatation and compaction (pressure solution) could lead to the transition from velocity strengthening to velocity weakening when increasing the temperature.

Based on the above, it is very difficult to point out one or more temperature dependent processes which are important for the velocity weakening process in limestone. To determine this, more research on this simulated limestone gouge must be executed.

5.2. Further recommendations

One of the main uncertainties is the role of Riedel shear bands in the limestone gouge. The displacement along and microphysical processes within an individual band are unknown. To resolve this problem at least partially, the experiment should be executed again with small adaptations. At several places, very thin gold foil or any other recognizable and very fragile material could be placed throughout the sample, perpendicular to the shearing direction. This foil will be sheared into the gouge and Riedel shear bands, making displacement calculations easier to accomplish.

Also pressurizing the starting material under the same stress as the sheared limestone gouges underwent could give new information. The material then becomes the real starting situation and (high resolution) microstructural analysis is easier to execute. Comparison will be less difficult and more realistic.

Calculations on the compaction strain rate due to pressure solution and strain rate due to twinning are useful to compare with the real microstructure. This can be done using the formulas and values provided by the research executed by Zhang et al. (in press). Knowing this, it is useful to continue the calculation on estimating the porosity and the coefficient of friction, so that it is possible to compare with the model discussed in this paper, and eventually to set up a new and better model fitting the limestone gouge at its best.

Acknowledgements

I would like to thank Chris Spiers and Martyn Drury for the supervision and funding of my thesis and all the time and advice put into it, so that I was able to finish this thesis in time. I would also like to thank Peter van Krieken for all the time behind the SEM and for preparing the samples for me. And last but not least, I would like to thank Professor Changrong He for providing the samples and the useful discussions we had during the HPT-China seminar and via the mail. My appreciation goes out for the people who also contributed to my thesis in any way, but whose name was not mentioned above.

References

Billi, A. (in press). Microtectonics of low-P low-T carbonate fault rocks. *Journal of Structural Geology xxx*, 1-11.

Bos, B. and Spiers, C.J. (2002). Frictional-viscous flow of phyllosilicate-bearing fault rock: Microphysical model and implications for crustal strength profiles. *Journal of Geophysical Research 107*, B22028, doi: 10.1029/2001JB000301.

Brace, W.F. and Byerlee, J.D. (1966). Stick slip as a mechanism for earthquakes. *Science 153*, 990-992.

Burkhard, M. (1993). Calcite twins, their geometry, appearance and significance as stress markers and indicators of tectonic regime: a review. *Journal of Structural Geology 15*, 351-368.

de Bresser, J.H.P. and Spiers, C.J. (1990). High-temperature deformation of calcite single crystals by r+ and f+ slip. *Geological Society 54*, 285-298.

de Bresser, J.H.P. and Spiers, C.J. (1997). Strength characteristics of the r, f, and c slip systems in calcite. *Tectonophysics 272*, 1-23.

Dieterich, J.H. (1979). Modeling of Rock Friction: 1. Experimental results and constitutive equations. *Journal of Geophysical Research 84*, 2161-2168.

Dunning, J., Douglas, B., Miller. And McDonald, S. (1994). The Role of the Chemical Environment in Frictional Deformation: Stress Corrosion Cracking and Comminution. *Pure and Applied Geophysics 143,* 151-178.

Ferrill, D.A., Morris, A.P., Evans, M.A., Burkhard, M., Groshong Jr., R.H. and Onasch, C.M. (2004). Calcite twin morphology: a low-temperature deformation geothermometer. *Journal of Structural Geology 28*, 1521-1529.

Fredrich, J.T. and Evans, B. (1989). Micromechanics of the Brittle to Plastic Transition in Carrara Marble. *Journal of Geophysical Research 94*, 4129-4145.

Han, R., Shimamoto, T., Hirose, T., Ree, J-H. and Ando, J-i. (2007a). Ultralow Friction of Carbonate Faults Caused by Thermal Decomposition. *Science 316*, 878-881.

Han, R., Shimamoto, T., Ando, J-i. and Ree, J-H. (2007b). Seismic slip record in carbonate-bearing fault zones: An insight from high-velocity friction experiments on siderite gouge. *Geology 35*, 1131-1134.

Han, R., Hirose, T. and Shimamoto, T. (2010). Strong velocity weakening and powder lubrication of simulated carbonate faults at seismic slip rates. *Journal of Geophysical Research 115*, B03415, doi: 10.1029/2008JB006136.

He, C., Yao, W., Wang, Z. and Zhou, Y. (2006). Strength and stability of frictional sliding of gabbro gouge at elevated temperatures. *Tectonophyisics 427*, 217-229.

Heilbronner, R. and Keulen, N. (2006). Grain size and grain shape analysis of fault rocks. *Tectonophysics 427*, 199-216.

Katz, Y., Weinberger, R. and Aydin, A. (2004). Geometry and kinematic evolution of Riedel shear structures, Capitol Reef National Park, Utah. *Journal of Structural Geology 26*, 491-501.

Keulen, N., Heilbronner, R., Stünitz, H., Boullier, A. and Ito, H. (2007). Grain size distributions of fault rocks: A comparison between experimentally and naturally deformed granitoids. *Journal of Structural geology 29*, 1282-1300.

Kolymbas, D. (2009). Kinematics of shear bands. *Acta Geotechnica 4*, 315-318.
Lee, R.H. (1995). Coatings and Alternatives for SEM Microscopy. Presented at INTER/MICRO'93, Chicago, IL.

Marone, C. and Scholz, C.H. (1989). Particle-size distribution and microstructures within simulated fault gouge. *Journal of Structural Geology 11*, 799-814.

Marone, C. (1998). Laboratory-derived friction laws and their application to seismic faulting. *Annual Reviews Earth and Planetary Science Letters 26*, 643-696.

Mizoguchi, K., Hirose, T., Shimamoto, T. and Fukuyama, E. (2009). High-velocity frictional behaviour and microstructure evolution of fault gouge obtained from Nojima fault, southwest Japan. *Tectonophysics 471*, 285-296.

Niemeijer, A. (2006). Effects of Pressure Solution and Phyllosilicates on the Slip and Compaction Behaviour of Crustal Faults. *Geologica Ultraiectina 255* (PhD thesis). Utrecht University, department of Earth Sciences.

Niemeijer, A.R. and Spiers, C.J. (2006). Velocity dependence of strength and healing behaviour in simulated phyllosilicate-bearing fault gouge. *Tectonophysicis 427*, 231-253.

Niemeijer, A.R. and Spiers, C.J. (2007). A microphysicial model for strong velocity weakening in phyllosilicate-bearing fault gouge. *Journal of Geophysical Research 112*, B10405, doi: 10.1029/2007JB005008.

Passchier, C.W. and Trouw, R.A.J. (1998). Microtectonics. 2nd corrected reprint. Springer-Verlag Berlin Heidelberg.

Riedel, W. (1929). Zur Mechanik Geologischer Brucherscheinungen. *Zentral-blatt fur Mineralogie, Geologie und Paleontologie B*, 354-368.

Rowe, K.J. and Rutter, E.H. (1990). Palaeostress estimation using calcite twinning: experimental calibration and application to nature. *Journal of Structural Geology 12*, 1-17.

Rutter, E.H. (1983). Pressure solution in nature, theory and experiment. *Journal of the Geological Society 140*, 725-740.

Sammis, C.G., Osborne, R.H., Anderson, J.L., Banerdt, M. and White, P. (1986). Self-Similar Cataclasis in the Formation of Fault Gouge. *Pure and Applied Geophysics 124*, 53-78.

Sammis, C.G., King, G. and Biegel, R.L. (1987). The Kinematics of Gouge Deformation. *Pure and Applied Geophysics 125*, 777-812.

Sammis, C.G. and Biegel, R.L. (1989). Fractals, Fault-Gouge, and Friction. *Pure and Applied Geophysics 131*, 255-271.

Storti, F., Billi, A. and Salvini, F. (2003). Particle size distribution in natural carbonate fault rocks: insights for non-self-similar cataclasis. *Earth and Planetary Science Letters 206*, 173-186.

Storti, F., Balsamo, F., Salvini, F. (2007). Particle shape evolution in natural carbonate granular wear material. *Terra Nova 19*, 344-352.

Stünitz, H., Keulen, N., Hirose, T. and Heilbronner, R. (2010). Grain size distribution and microstructures of experimentally sheared granitoud gouge at coseismic slip rates - Criteria to distinguish seismic and aseismic faults? *Journal of Structural Geology 32*, 59-69.

Sulem, J. and Famin, V. (2009). Thermal decomposition of carbonates in fault zones: Slip-weakening and temperature-limiting effects. *Journal of Geophysical Research 114*, B03309, doi:10.1029/2008JB006004.

Verberne, B.A., He, C. and Spiers, C.J. (in press). Frictional Properties of Sedimentary Rocks and Natural Fault Gouge from the Longmenshan Fault Zone, Sichuan, China. *Bulletin of the Seismological Society of America.*

Wang, J.H. (1996). Velocity-Weakening Friction as a Factor in Controlling the Frequency-Magnitude Relation of Earthquakes. *Bulletin of the Seismological Society of America 86*, 701-713.

Wilson, B., Deweres, T., Reches, Z. and Brune, J. (2005). Particle size and energetics of gouge from earthquake rupture zones. *Nature 434*, 749- 752.

Zhang, X. and Spiers, C.J. (2005). Compaction of granular calcite by pressure solution at room temperature and effects of pore fluid chemistry. *International Journal of Rock Mechanics & Mining Sciences 42*, 950-960.

Zhang, X., Spiers, C.J. and Peach, C.J. (in press). Compaction creep of wet granular calcite by pressure solution at 28 to 150°C.